Dalton Transactions

Accepted Manuscript

ROYAL SOCIETY OF CHEMISTRY

www.rsc.org/dalton

Self-assembled Cu(II) and Ni(II) metallamacrocycles formed from 3,3,3′,3′-tetrabenzyl-1,1′-aroylbis(thiourea) ligands: DNA and protein binding studies, and cytotoxicity of trinuclear complexes

Nagamani Selvakumaran[a], Nattamai S.P. Bhuvanesh[b] and Ramasamy Karvembu*[a]

Self-assembled metallamacrocyclic Cu(II) and Ni(II) complexes of the types $[Cu(L1\text{-}O,S)]_3$ (**1**), $[Ni(L1\text{-}O,S)]_3$ (**2**), $[Cu(L2\text{-}O,S)]_2$ (**3**) and $[Ni(L2\text{-}O,S)]_2$ (**4**) [H_2L1 = 3,3,3′,3′-tetrabenzyl-1,1′-terephthaloylbis(thiourea) and H_2L2 = 3,3,3′,3′-tetrabenzyl-1,1′-isophthaloylbis(thiourea)] were synthesized and characterized by analytical, spectroscopic (UV-Vis, FT-IR, Mass, ^1H & ^{13}C NMR and EPR) and single crystal X-ray diffraction techniques. The crystal structures of $[Ni(L1\text{-}O,S)]_3$ and $[Cu(L2\text{-}O,S)(Py)]_2$ showed the formation of self-assembled 3:3 and 2:2 metallamacrocyclic Cu(II) and Ni(II) complexes respectively. The binding affinity and binding mode of the trinuclear complexes toward CT DNA were determined by UV-Vis spectrophotometric titrations and fluorescent indicator displacement (FID) assay. The interaction of the ligand (H_2L1) and the complexes (**1** and **2**) with BSA was investigated using UV-Vis and fluorescence spectroscopic methods. Absorption and emission spectral studies indicate that the complexes **1** and **2** interact with CT DNA and BSA protein more strongly than their parent ligand. Both the complexes (**1** and **2**) cleaved the pBR 322 plasmid DNA in the absence of an external agent. Complex **1** [IC50 = 22.36 (A549) and 10 μM (MCF7)] exhibited higher cytotoxicity than cyclophosphamide against A549 and MCF7 cancer cell lines. The IC50 value of **2** (29.24) is higher in A549 cell line and slightly lower (18.04) in MCF7 cell line than that of cyclophosphamide [IC50 = 41.84 (A549) and 11.89 μM (MCF7)].

[a]*Department of Chemistry, National Institute of Technology, Tiruchirappalli 620 015, India, E-mail: kar@nitt.edu*
[b]*Department of Chemistry, Texas A&M University, College Station, TX 77842, USA*

Electronic Supplementary Information (ESI) available: ^1H and ^{13}C NMR spectra of ligands (H_2L1 and H_2L2) and complex **2**. CCDC reference numbers 1000649-1000652. For ESI and crystallographic data in CIF or other electronic format see DOI:

Introdu ction

The coord ination chemistry of bipodal aroylthiourea derivatives is very interesting, because symmetrical bipodal derivatives with two S,O chelating moieties such as 3,3,3′,3′-tetraalkyl-1,1′-aroylbis(thiourea) are best suitable for the synthesis of multinuclear complexes.[1-4] These molecules appeared to be preprogrammed to form, through self-assembly, discrete metallamacrocyclic complexes with metal ions such as Cu^{II}, Ni^{II}, Pd^{II} and Pt^{II}.[2,3] The metallamacrocyclic complexes with well-defined metal to ligand ratios are exclusively formed depending on the relative substitution positions of the aroylthiourea moieties on the phenyl spacer. Particularly, *meta* substituted phthaloylthiourea ligands are able to form 2:2 self-assembled metallamacrocyclic complexes and *para* substitution leads to 3:3 metallamacrocycles. In all the structurally characterized bi or trinuclear complexes of this type, the original coordination mode of the bidentate benzoylthioureas *i.e.* square planar coordination with *cis* arrangement of the donor atoms is maintained. Some reports have shown that octahedral adducts of both 2:2 and 3:3 Ni(II) metallamacrocycles can be obtained by the addition of pyridine, which display interesting host-guest chemistry.[5] This illustrates the potential of such essentially planar metallamacrocyclic Ni(II) complexes to function as secondary building blocks for further assembly into three dimensional higher ordered structures using suitable linker molecules. In another example Pt(IV) metallamacrocyclic complexes of the bipodal 3,3,3′,3′-tetraalkyl-1,1′-phenylenedicarbonylbis(thioureas) were readily synthesized by the oxidative addition of dihalogens to the Pt(II) complexes of these ligands.[6] The square planar 2:2 metallamacrocyclic complexes possess two available axial coordination sites per metal atom; these compounds could be expected to act as 4-connected nodes for the purpose of assembly into 1D and 2D polymeric arrays.[4] Nguyen *et al* recently reported 2:2 oxorhenium(V) complexes with 3,3,3′,3′-tetraalkyl-1,1′-isophthaloyl bis(thiourea) ligands, in which each Re is coordinated by two bidentate O,S moieties. Two of such compounds can dimerize when the axial methoxido co-ligand is replaced by hydroxido ligands with subsequent condensation.[7]

The increasing interest in using macrocycles and their coordination compounds as artificial restriction enzymes for binding, cleaving DNA and RNA has prompted us to investigate the application of macrocyclic Cu(II) and Ni(II) complexes in this area. In the past few years, multinuclearity has been one of the successful strategies to increase the efficiency and selectivity of the metallonucleases due to the potential cooperative effects between the metal centers,[8-10] which stimulated us to design and synthesize multinuclear complexes to

evaluate and understand the factors on the DNA binding properties. A number of proposals has been put forth describing the reactivity of DNA with mononuclear Cu and Ni complexes.[11,12] Compared to the number of studies dealing with the mononuclear complexes, studies on multinuclear complexes are less.[13-19] Karlin and co-workers have already demonstrated that multinuclear Cu complexes containing pyridyl ligands have more effective DNA cleavage abilities than their mononuclear analogues.[20] Cu and Ni are the most essential elements for the biological systems and present in the trace quantities. Ni(II) complexes of macrocyclic ligands containing mixed donors have attracted much attention because they are used as a model for nickel centered enzymes such as bifunctional carbon monoxide dehydrogenase/acetyl-CoA synthase, nickel containing superoxide dismutase, urease and phosphatase.[21-24] Metal ion mediated hydrolysis of phosphate esters is a common catalytic pathway in nucleic acid biochemistry.[25] It was reported that dinuclear Ni(II) complexes are active catalysts for phosphate hydrolysis.[26] The symmetrical and unsymmetrical macrocyclic Ni(II) complexes containing *o*-alkyloxime moiety and alkyl/aromatic diamines, exhibited potential intercalative binding and electrostatic interaction with DNA base pairs.[27] Polyaza macrobicyclic dinickel(II) complexes showed intercalative mode of interaction with CT DNA.[28]

Cu has been found to possess high DNA binding affinity.[29] Analogously to what has been widely illustrated for cisplatin,[30] a crystal structure describing formation of an adduct between $CuCl_2$ and DNA was published in 1991, in which copper bound to the guanine N7 residue.[31] This binding was dependent on copper complex size, electron affinity, and geometry of the formed adduct, inducing an irreversible modification of the DNA conformational structure. According to these observations, a large number of Cu complexes has been tested as DNA-targeting metallo drugs. Cu complexes with various types of ligands act as an anticancer agents against approximately ninety cancer cell lines. For some classes of Cu derivatives, the ability to bind DNA has been well established and documented.[32] However, only a few attempts have been made to understand the binding abilities of macrocyclic Cu(II) complexes with DNA. It has been reported that tetraaza and hexaaza macrocyclic Cu(II) complexes possess anti-HIV activity, and DNA binding and cleavage properties.[33,34] The binuclear macrocyclic Cu(II) complexes are avid binders to CT DNA and it displayed significant oxidative cleavage of circular plasmid pBR 322 DNA in the presence of mercapto ethanol using the singlet oxygen as a reactive species.[35] Piperazine and bipyridyl or phenanthroline moieties coordinated binuclear Cu(II) complexes bind to double-stranded

DNA in the major groove mode and remarkably cleave supercoiled plasmid DNA.[36] Binuclear macrocyclic Cu(II) complexes containing phenanthroline and dicarboxylate ligands showed anaerobic DNA cleavage activity in red light.[37] DNA binding, DNA hydrolysis and phosphatase-like activities of polyazamacrobicyclicdicopper(II) complexes are reported.[38] Therefore, extensive studies on the interaction of macrocyclic Cu and Ni complexes with DNA are necessary. Herein we report the results of structural analysis of 3,3,3′,3′-tetrabenzyl-1,1′-aroylbis(thiourea) ligands and their self-assembled 2:2 and 3:3 Cu(II) and Ni(II) macrocyclic complexes and DNA/protein binding studies of 3:3 trinuclear complexes.

Experimental

Materials and physical measurements

Solvents were purified according to the standard procedures. Elemental analyses were performed with a Vario EL-III elemental analyzer. UV-Vis spectra were recorded on a Shimadzu-2600 spectrophotometer operating in the range of 200-900 nm. Emission spectra were recorded on a Jasco V-630 spectrophotometer using 5% DMF in buffer as the solvent. EPR spectra were recorded with a Bruker ESP 300E X-band spectrometer at 77 K in CH_2Cl_2 solution. FT-IR spectra were recorded in the 4000-400 cm^{-1} region (KBr discs) on a Nicolet iS5 FT-IR spectrophotometer. ^1H and ^{13}C NMR spectra were recorded on a Bruker AM 400 spectrometer. MALDI-TOF mass spectra were recorded on a 4800-Applied Bio System mass spectrometer using TiO_2 matrix.

Synthesis of 3,3,3′,3′-tetrabenzyl-1,1-terephthaloyl/isophthaloylbis(thiourea) Terephthaloyl/isophthaloyl dichloride (4.0604 g, 0.020 mole) dissolved in acetone (120 mL) was placed in a dropping funnel and added drop wise with stirring to dry potassium thiocyanate (3.8872 g, 0.040 mole) dissolved in acetone (120 mL) under N_2 atmosphere. During the addition, a pale yellow precipitate was formed. The mixture was stirred for 1 h at room temperature. Dibenzylamine (7.8912 g, 0.040 mole) dissolved in acetone (120 mL) was added drop wise to the reaction mixture. The mixture was stirred for another 2 h. A pale orange solution with an off-white precipitate was observed. The mixture was transferred to a large beaker containing 500 mL of water. The precipitate got dissolved in water. Acetone in the mixture was allowed to evaporate. After 48 h, off-white solid product was formed, which was purified by column chromatography using ethylacetate/hexane mixture (2:8) as an eluent.

3,3,3′,3′-Tetrabenzyl-1,1-terephthaloylbis(thiourea) (H_2L1). Yield: 73%. Elemental analyses found: C, 70.28; H, 5.17; N, 8.29; S, 9.36%. $C_{38}H_{34}N_4O_2S_2$: Calc. C, 71.00; H, 5.33; N, 8.72; S, 9.98%. UV-Vis (5% DMF in buffer, λ_{max}, nm): 242, 302. FT-IR

(KBr, cm^{-1}): 3202 (NH), 1698 (C═O), 1229 (C═S). ^1H NMR (400 MHz, DMSO-d_6, ppm): 4.79 (s, 4H, CH_2), 5.24 (s, 4H, CH_2), 7.18 (d, J = 6.8 Hz, 4H), 7.32-7.41 (m, 12H), 7.48 (d, J = 7.2 Hz, 4H), 7.89 (s, 4H), 11.14 (s, 2H, NH). ^{13}C NMR (100 MHz, DMSO-d_6, ppm): 55.3, 56.2 (CH_2), 127.7, 127.9, 128.4, 128.7, 128.9, 129.2, 135.4, 136.2, 136.4 (C_6H_5), 164.3 (C═O), 183.4 (C═S). MALDI-TOF MS: MW, 642.8446; m/z: 196.0152 $[N\text{-}(benzyl)_2]^+$, 445.9832 $[M–H–N\text{-}(benzyl)_2]^+$, 680.9713 $(M–H+K)^+$.

3,3,3′,3′-Tetrabenzyl-1,1-isophthaloylbis(thiourea) (H_2L2). Yield: 65%. Elemental analyses found: C, 70.36; H, 5.16; N, 8.60; S, 9.75%. $C_{38}H_{34}N_4O_2S_2$: Calc. C, 71.00; H, 5.33; N, 8.72; S, 9.98%. UV-Vis (5% DMF in buffer, λ_{max}, nm): 235, 292. FT-IR (KBr, cm^{-1}): 3123 (NH), 1697 (C═O), 1234 (C═S). ^1H NMR (400 MHz, DMSO-d_6, ppm): 4.69 (s, 4H, CH_2), 5.21 (s, 4H, CH_2), 7.17 (d, J = 7.2 Hz, 4H), 7.27-7.47 (m, 16H), 7.61 (t, J = 8.0 Hz, 1H), 8.03 (d, J = 7.6 Hz, 2H), 8.33 (s, 1H), 10.99 (s, 2H, NH). ^{13}C NMR (100 MHz, DMSO-d_6, ppm): 55.4, 56.1 (CH_2), 127.7, 128.4, 128.6, 129.3, 129.4, 132.4, 133.3, 135.3, 136.0 (C_6H_5), 164.3 (C═O), 183.3 (C═S). MALDI-TOF MS: MW, 642.8446; m/z: 665.0071 $(M+2Na)^+$, 680.9692 $(M–H+K)^+$.

Synthesis of Cu(II) and Ni(II) complexes

$[Cu(L1\text{-}O,S)]_3$ (1). $Cu(OAc)_2{\cdot}H_2O$ (0.1998 g, 0.001 mole) was dissolved in 15 mL of DMF and the DMF solution of H_2L1 (0.6428 g, 0.001 mole) was added. The reaction mixture was stirred for 2 h at room temperature and kept at cold condition. After three days, black colored crystalline solid was formed and the precipitate was filtered off, washed with cold MeOH, and dried in *vacuum*. Yield: 85%. Elemental analyses found: C, 64.77; H, 4.46; N, 7.82; S, 9.02%. $C_{114}H_{96}N_{12}Cu_3O_6S_6$: Calc. C, 64.81; H, 4.58; N, 7.95; S, 9.10%. UV-Vis (5% DMF in buffer, $\lambda_{mand\ Ni(II)ax}$, nm): 252, 316, 365. UV-Vis (solid state, λ_{max}, nm): 281, 379, 504, 587. FT-IR (KBr, cm^{-1}): 1521 (C┈┈O), 1205 (C┈┈S), EPR (X band, 77 K, ν = 9.78 GHz): g, 2.1769.

$[Ni(L1\text{-}O,S)]_3$ (2). $Ni(OAc)_2{\cdot}4H_2O$ (0.2488 g, 0.001 mole) was dissolved in 15 mL of DMF and the DMF solution of H_2L1 (0.6428 g, 0.001 mole) was added. The reaction mixture was stirred for 2 h at room temperature and kept at cold condition. After three days, brown colored crystalline solid was formed and the precipitate was filtered off, washed with cold MeOH, and dried in *vacuum*. Yield: 78%. Elemental analyses found: C, 65.02; H, 4.48; N, 7.93; S, 9.05%. $C_{114}H_{96}N_{12}Ni_3O_6S_6$: Calc. C, 65.25; H, 4.61; N, 8.01; S, 9.17%. UV-Vis (5% DMF in buffer, λ_{max}, nm): 269, 318, 398. UV-Vis (solid state, λ_{max}, nm): 291, 391, 511, 541. FT-IR (KBr, cm^{-1}): 1520 (C┈┈O), 1206 (C┈┈S). ^1H NMR (400 MHz, $CDCl_3$, ppm): 4.91 (s,

12H, CH_2), 4.99 (s, 12H, CH_2), 7.21-7.35 (m, 60H), 8.10 (s, 12H). ^{13}C NMR (100 MHz, $CDCl_3$, ppm): 55.4, 56.1 (CH_2), 127.6, 127.7, 127.9, 129.1, 135.4, 136.3, 139.2 (C_6H_5), 173.3 (C=O), 175.0 (C=S).

[Cu(L2-O,S)]$_2$ (3). $Cu(OAc)_2{\cdot}H_2O$ (0.1998 g, 0.001 mole) was dissolved in 15 mL of MeOH and the MeOH/DMF (2:1) mixture solution of H_2L2 (0.6428 g, 0.001 mole) was added. The reaction mixture was stirred for 2 h at room temperature. The green precipitate formed was filtered off, washed with cold MeOH, and dried in *vacuum*. Yield: 68%. Elemental analyses found: C, 64.78; H, 4.46; N, 7.90; S, 9.01%. $C_{76}H_{64}N_8Cu_2O_4S_4$: Calc. C, 64.81; H, 4.58; N, 7.95; S, 9.10%. UV-Vis (solid state, λ_{max}, nm): 279, 379, 485, 585. FT-IR (KBr, cm^{-1}): 1514 (C=O), 1210 (C=S). MALDI-TOF MS: MW, 1408.7496; m/z: 1407.9264 $(M-H)^+$, 1408.9353 $(M)^+$, 1409.9398 $(M-H)^+$, 1430.9017 $(M-H+Na)^+$. EPR (X band, 77 K, ν = 9.78 GHz): g, 2.1751.

[Ni(L1-O,S)]$_2$ (4). $Ni(OAc)_2{\cdot}4H_2O$ (0.2488 g, 0.001 mole) was dissolved in 15 mL of MeOH and the MeOH/DMF (2:1) mixture solution of H_2L2 (0.001 mole) was added. The reaction mixture was stirred for 2 h at room temperature. The pink colored precipitate formed was filtered off, washed with cold MeOH, and dried in *vacuum*. Yield: 63%. Elemental analyses found: C, 65.12; H, 4.58; N, 7.88; S, 9.10%. $C_{76}H_{64}N_8Ni_2O_4S_4$: Calc. C, 65.25; H, 4.61; N, 8.01; S, 9.17%. UV-Vis (solid state, λ_{max}, nm): 279, 388, 522, 628. FT-IR (KBr, cm^{-1}): 1511 (C=O), 1208 (C=S). MALDI-TOF MS: MW, 1399.0376; m/z: 1399.1179 $(M)^+$, 1437.0808 $(M-H+K)^+$.

Crystal structure determination

Single crystal X-ray diffraction data for H_2L1, H_2L2 and **3(Py)$_2$** were collected using Bruker APEX2 (MoKα), and for **2** using a Bruker GADDS (CuKα) diffractometers.[39] For the latter data, CELL_NOW[40] was used for unit cell determination. Integrated intensity information for each reflection was obtained by reduction of data frames with APEX2.[41] SADABS was employed to correct the data for absorption effects.[42] The structures were solved by direct methods (SHELXS) and refined (SHELX-97, weighted least squares refinement on F^2) using APEX2, and OLEX2, respectively.[43],[44] Non-hydrogen atoms were refined with anisotropic thermal parameters. The structures were refined (weighted least squares on F^2) to convergence.[43] The absence of additional symmetry and/or voids were verified with PLATON.[45] The crystallographic data and the results of refinements are summarized in Tables 1–4.

DNA binding experiments

For absorption spectral studies, DNA samples were dissolved in 50 mM NaCl/5 mM Tris HCl (pH 7.2) solution. CT DNA solution displayed a UV absorbance ratio at 260 and 280 nm (*A*260/*A*280) of *ca.* 1.9:1, indicating that the CT DNA was sufficiently in protein free form. The concentration of the nucleic acid solutions was determined by UV absorbance at 260 nm after 1:100 dilutions. The extinction coefficient at 260 nm was taken as 6600 $M^{-1}cm^{-1}$.[46] Stock solutions were stored at 4 °C and used within 4 days. 0-50 μL of CT DNA was added to the complex solution. The spectra were recorded after equilibration for 3 minutes, allowing the compounds to bind to the CT DNA. Concentrated stock solutions were prepared by dissolving calculated amounts of the compounds (H_2L1, **1** and **2**) in a 5% DMF/5 mM Tris−HCl/50 mM NaCl buffer to required concentrations for all the experiments.

The competitive studies of each compound with EB have been investigated by using florescence spectroscopy. The excitation wavelength was fixed, and emission range was adjusted before measurements. DNA was pretreated with ethidium bromide (EB) in the 1:1 ratio for 15 minutes. The compounds were then added to this mixture, and their effect on the emission intensity was measured. The Stern−Volmer equation is used to evaluate the apparent binding constant (K_{app}) and quenching constant (K_q) values of the compounds. The changes in fluorescence intensities at 596 nm (510 nm excitation) of EB bound to DNA were recorded with an increasing amount of the compounds until maximum reduction in the intensity of fluorescence occurred.

Viscosity experiments were carried out using a semi micro viscometer maintained at 27 °C in a thermostatic water bath. DNA samples (0.5 mM) were prepared by sonication in order to minimize complexities arising from DNA flexibility.[47] Flow time was measured three times for each sample and an average flow time was calculated. The values of relative specific viscosity (η/η^0), where η is the relative viscosity of DNA in the presence of the complex and η^0 is the relative viscosity of DNA alone, were plotted against 1/R (1/R = [compound]/[DNA]). Relative viscosity (η^0) values were calculated from the observed flow time of the DNA solution (t) corrected for the flow time of the buffer alone (t^0), using the expression $\eta^0 = (t - t^0)/t^0$.[48,49]

DNA cleavage experiment

A mixture of Tris buffer (5 mM Tris-HCl/50 mM NaCl buffer, pH 7.2), pBR 322 plasmid DNA (200 μg/mL) and different amounts of the complexes were incubated for 2 h at 37°C. A dye solution (0.05% bromophenol blue and 5% glycerol) was added to the reaction mixture

prior to electrophoresis. The samples were then analyzed by 1.5% agarose gel electrophoresis [Tris-HCl/Boric acid/EDTA (TBE) buffer, pH 8.0] for 3 h at 60 mV. The gel was stained with 0.5 μg mL^{-1} ethidium bromide, visualized by UV light, and photographed. The extent of cleavage of the pBR 322 DNA was determined by measuring the intensities of the bands using AlphaImager HP instrument.

Protein binding experiments

Quenching of the emission of tryptophan residues of BSA was performed using the compounds (H_2L1, **1** and **2**) as quenchers. To a solution of BSA in phosphate buffer (pH 7.2), increments of the quenchers were added, and the emission signals at 341 nm (280 nm excitation) were recorded after each addition of the quencher. The excitation and emission slit widths and scan rates were constantly maintained for all the experiments. Concentrated stock solutions of test compounds were prepared by dissolving them in DMF and diluted suitably with phosphate buffer to get required concentrations. 2.5 mL of BSA solution (1 μM) was titrated by successive additions of a 5 mL stock solution of test compounds (10^{-4} M) using a micropipette. Synchronous fluorescence spectra were also recorded using the same concentration of BSA and test compounds as mentioned above with two different Δλ (difference between the excitation and emission wavelengths of BSA) values such as 15 and 60 nm.

Cytotoxic activity

Cell culture

A549 (human lung cancer cell line) and MCF7 (human breast cancer cell line) were obtained from the National Centre for Cell Science (NCCS), Pune, and maintained in Roswell Park Memorial Institute (RPMI) medium containing 10% fetal bovine serum (FBS). For evaluation of the cytotoxicity, cells were seeded on a 96 well plate with a density of 1×10^4 cells/cm^2. Normal cells of HDF (human dermal fibroblast cell line) were maintained in Human Dermal Fibroblast medium (HDF-growth medium) provided by Promo Cell, Germany.

Assessment of cytotoxicity

Cytotoxicity of ligand (H_2L1) and complexes (**1** and **2**) was evaluated by using the MTT [3-(4,5-dimethylthiazole-2-yl)-2,5-diphenyltetrazolium] assay.[50] This colorimetric test is based on the selective ability of viable cells to reduce the tetrazolium component of MTT into purple coloured formazan crystals. Stock solutions of the samples were freshly prepared and diluted with cell culture medium to the desired concentrations (10, 50, 100 and 200 μg/μL). The compounds with different concentrations were added and incubated with phosphate

buffer saline (PBS) resuspended cells, after attaining 90% confluency. Cells in media devoid of compound acted as the negative control and wells treated with Triton X-100 as the positive control for a period of 24 h. 5 mg of MTT (Sigma) was dissolved in 1 mL of PBS and filter sterilized. 10 μL of the MTT solution was further diluted to 100 μL with 90 μL of serum and phenol red free medium. The cells were incubated with 100 μL of the above solution for 4 h to form formazan crystals by mitochondrial dehydrogenates. 100 μL of the solubilisation solution (10% Triton X-100, 0.1 N HCl and isopropanol) was added to each well and incubated at room temperature for 1 h to dissolve the formazan crystals. The absorbance of the solution was measured at 570 nm using a Beckmann Coulter Elisa plate reader (BioTek Power Wave XS).[51] Triplicate samples were analyzed for each experiment.

Results and discussion

Bipodal 3,3,3′,3′-tetrabenzyl-1,1′-aroylbis(thioureas) (H_2L1 and H_2L2) were prepared from isophthaloyl/terephthaloyl chloride, KSCN and dibenzylamine (Scheme 1) and used as pre-programmed chelating ligands to form square planar metallamacrocyclic Cu(II) and Ni(II) complexes *via* self-assembly. Metal to ligand stoichiometries of 2:2 and 3:3 can be achieved by using *meta* or *para* substituted ligands, respectively (Schemes 2 and 3). All the complexes have been obtained in good yields and characterized by analytical and spectral techniques. The X-ray crystal structure of **2** reveals trimetallic composition and related copper complex (**1**) is suggested to possess the same structure, which is supported by analytical and spectral data. As **3** and **4** possess poor solubility in most of the common organic solvents, pyridine was used as solvent to grow the crystals. Complex **3** crystallized with the coordination of one pyridine to each Cu center [**3**$(Py)_2$], which lead to square pyramidal structure for 2:2 metallamacrocyclic complex. We could not get suitable crystals for **4** but structure of which has been confirmed by its mass spectra.

Characterization

Spectral methods

Electronic spectra of the ligands (H_2L1 and H_2L2) showed two strong absorption bands in the regions 235-242 and 261-292 nm, which are assigned to $\pi \rightarrow \pi^*$ and $n \rightarrow \pi^*$ transitions respectively. In the Cu(II) and Ni(II) complexes of H_2L1, three bands were observed in the regions 252-269, 316-318 and 365-398 nm. The high intensity bands in the regions 252-269 and 316-318 nm correspond to intra ligand transitions. A less intense band at 365-398 nm has been assigned to ligand to metal charge transfer process. The $d \rightarrow d$ transition of all the Cu(II) and Ni(II) complexes was observed in the DRS mode at 585-587 and 541-628 nm

respectively. Similar assignments have been made for other square planar Ni(II) and Cu(II) complexes.[52]

The FT-IR spectra of the ligands (H_2L1 and H_2L2) showed the absorption band for the stretching of N−H at 3202-3123 cm^{-1}, which was absent in the complexes indicating deprotonation of the N−H group. A strong band observed in the region 1698-1697 cm^{-1} in the FT-IR spectra of the ligands was assigned to the C═O stretching vibration. This band was shifted to the lower frequency range of 1521-1511 cm^{-1} in the spectra of the complexes (**1-4**), consistent with the coordination of O to the metal ion. The characteristic band for C═S appeared at 1234-1229 cm^{-1} in the spectra of H_2L1 and H_2L2 was shifted to lower frequency (1210-1205 cm^{-1}) on complexation, indicating involvement of S in coordination.

^1H and ^{13}C NMR spectra of H_2L1, H_2L2 and **2** are shown in Figs. S1-S6. The signal for the N−H proton that appeared as a singlet at 11.14 ppm in the ^1H NMR spectrum of H_2L1 was not present in the spectrum of its nickel(II) complex (**2**). This supports the deprotonation of N−H group as also revealed from the FT-IR spectra. The characteristic signals of the aromatic protons present in **2** were observed in the region 7.16-8.33 ppm as multiplets. The signals due to methylene protons were observed in the region 4.71-5.24 ppm. In the ^{13}C NMR spectrum of **2**, thiocarbonyl and carbonyl carbon signals were found in the regions 175.0 and 173.3 ppm, respectively. These resonances are entirely different from those in H_2L1 (C═O, 164.3 and C═S, 183.3 ppm). The resonances for aromatic and aliphatic carbons were observed in the regions 127.6-139.2 and 55.4-56.1 ppm respectively.

The X-band EPR spectra of the Cu(II) complexes (**1** and **3**), recorded in CH_2Cl_2 at liquid N_2 temperature (70 K) showed an intense signal in the high field, which is isotropic due to the tumbling motion of the molecules (Fig. 1). They are characteristic of Cu^{2+} and exhibited 'g' values of 2.1751 and 2.1769 for **1** and **3** respectively. These values ($g > 2$) indicate that the ground state of Cu(II) is predominantly $dx^2–y^2$.[53]

MALDI-TOF MS has been proven itself to be useful method for the analysis of macromolecules. Figs. 2 and 3 represent the mass spectra of complexes **3** and **4** respectively. The $[M^+]$ and $[M+Na]^+$ peaks were detected at *m/z* 1408.9353 and 1430.9017 in the mass spectrum of **3**. The remaining two peaks correspond to deprotonated (*m/z* 1407.9264) and protonated (*m/z* 1409.9398) species of the complex. There are two major peaks arising from complex **4** at *m/z* 1399.1179 and 1437.0808, which are due to the molecular ion peak and $[M–H+K]^+$.

X-ray crystallography

The molecular structure of the ligands (H_2L1 and H_2L2) and the complexes [**2** and **3**$(Py)_2$] with the atomic labeling schemes is shown in the Figs. 4-7. Crystal data and structure refinement details are provided in Tables 1 and 2. Selected bond lengths and bond angles are listed in Tables 3 and 4. Half a water molecule and one DMF moiety were found solvated per molecule of H_2L1. The H_2L2 adopts a U-shape as both pendent side arms of the 1,3-substituted benzene ring are oriented in the same direction. Whereas in the case of H_2L1 pendent side arms are opposite to each other.

The molecular structure of **2** is nearly planar 3:3 metallamacrocyclic assembly, with the aromatic rings of the terephthaloyl moiety are essentially coplanar with the coordination sphere of the Ni(II) centers. The coordination sphere of each Ni(II) ion in complex **2** is distorted significantly from ideal square planar geometry [for instance S(1)-Ni(1)-S(2F) 83.63(6)°, O(1)-Ni(1)-O(2F) 85.35(14)°, O(2F)-Ni(1)-S(1) 175.89(12)° and O(1)-Ni(1)-S(2F) 172.17(12)°]. Structural analyses of **2** revealed that three dianionic bis(aroylthiourea) ligands (L1) coordinated to three Ni(II) centers in tetradentate fashion. Comparing the C–O [1.259(5) Å] and C–S [1.711(5) Å] bond lengths of **2** with H_2L1 [C–O, 1.2207(15) and C–S, 1.6710(14) Å], considerable elongation of these bonds was noted in the complex. On the other hand, N–C(O) [1.313(3) Å] and N–C(S) [1.351(3) Å] bond lengths of the chelate rings in **2** were short compared to the N–C bond distances of the corresponding ligand [N–C(O), 1.3486(15) and N–C(S), N–C(S) 1.4343(15) Å]. These results are consistent with the fact that the ligand underwent deprotonation during the reaction and coordinated to Ni(II) *via* O and S donor atoms. Further, there was a significant delocalization of π-electron density over the six atoms comprising the respective chelate rings in the complex. The value of τ_4 (0.085) suggests distorted square planar geometry for complex **2**.[54] The suitable single crystals of **3** were obtained from pyridine solution of the complex by diffusing acetone vapor. Consequently, one pyridine molecule was coordinated to each Cu(II) ion [**3**$(Py)_2$] as revealed from its crystal structure obtained from XRD data. The molecular structure of **3**$(Py)_2$ seems to be 2:2 metallamacrocyclic assembly, with the aromatic rings of the isopththaloyl moiety are essentially coplanar with the coordination sphere of the Cu(II) centers. The coordination behavior of the ligands in **3**$(Py)_2$ is very similar to that in **2**. The calculated τ_5 value of **3**$(Py)_2$ is 0.066 indicating square pyramidal structure.

DNA binding studies

UV-Vis absorption spectra

The intrinsic binding constant (K_b) values for the interaction of H_2L1, **1** and **2** with CT DNA are 1.52×10^4, 1.98×10^4 and 2.38×10^4, respectively (Table 5), which has been calculated from the absorption spectral titration data using the equation $[DNA]/(\varepsilon_a-\varepsilon_f) = [DNA]/(\varepsilon_b-\varepsilon_f) + 1/K_b(\varepsilon_b-\varepsilon_f)$, where [DNA] is the concentration of DNA in base pairs. The apparent absorption coefficients ε_a, ε_f, and ε_b correspond to A_{obsd}/[compound], the extinction coefficient for the free compound and the extinction coefficient for the compound in the fully bound form, respectively. The slope and the intercept of the linear fit of $[DNA]/[\varepsilon_a-\varepsilon_f]$ *versus* [DNA] plot give $1/[\varepsilon_a-\varepsilon_f]$ and $1/K_b[\varepsilon_b-\varepsilon_f]$, respectively. Fixed amounts of the test compounds were dissolved in DMF and utilized for titrations. When H_2L1 was subjected to CT DNA interaction, intensity of intra ligand transition band at 302 nm decreases slightly with small red shift (3 nm) (Fig. 8). In the UV spectrum of complex **1**, the band at 316 nm exhibited a significant hypochromism and substantial red shift (8 nm) upon the addition of CT DNA. During the incremental addition of CT DNA to complex **2**, the band due to intra ligand transition at 318 nm exhibited hypochromism with red shift. The results derived from the UV-Vis titration experiments suggest that all the compounds (H_2L1, **1** and **2**) can bind to DNA. However the complexes interact with CT DNA strongly than the corresponding bis(aroylthiourea) ligand. The K_b values of the compounds follow the order, H_2L1<**1**<**2** (Fig. 9).

Ethidium bromide displacement study

The binding of the compounds (H_2L1, **1** and **2**) to CT DNA was studied by evaluating the fluorescence emission intensity of the ethidium bromide bounded DNA (EB-DNA) upon the addition of the compounds. If the compounds added to the EB-DNA replace the bound EB, the emission intensity will be reduced. The fluorescence quenching of EB-DNA by compounds is shown in Fig. 10. The relative binding propensity of the compounds to CT DNA was determined by the classical Stern-Volmer equation[55,56] $F^o/F = 1 + K_q[Q]$, where F^o and F are the fluorescence intensities in the absence and the presence of the quencher, respectively. K_q is the linear Stern-Volmer quenching constant. Upon addition of the ligand and its complexes to EB-DNA, the emission intensity of EB bound DNA decreases. From the plot of these intensities against complex concentration (Fig. 11), the values of apparent DNA binding constant (K_{app}) were calculated using the equation $K_{EB}[EB] = K_{app}[complex]$, where

K_{EB} is 1.0×10^7 M^{-1}, the concentration of EB is 5 μM, and the concentration of the complex is that used to obtain a 50% reduction of fluorescence intensity of EB. The DNA binding ability of the compounds follows the order **2**>**1**>H_2L1, which is consistent with the results obtained from absorption spectral studies. The quenching and binding constants of the ligand and the Ni(II) and Cu(II) complexes suggested that the interaction of tested compounds with CT DNA should be of intercalation.[57]

Viscosity measurements

Since the relative specific viscosity (η/η^0) of DNA gives a measure of the increase in contour length associated with the separation of DNA base pairs caused by intercalation, a classical DNA intercalator like EB shows a significant increase in the viscosity of the DNA solutions (η and η^0 are the specific viscosities of DNA in the presence and absence of the test compounds, respectively). Lengthening of DNA helix occurs on intercalation as base pairs are separated to accommodate the binding compound leading to increase in DNA viscosity. The values of relative specific viscosities of CT DNA in the absence and presence of the compounds are plotted against [complex]/[DNA]. The relative viscosities of CT DNA bound to the ligand (H_2L1) and the complexes (**1** and **2**) increased with increasing compound concentration (Fig. 12) similar to some known intercalators,[58] indicative of a classical intercalation.

Nuclease activity

The cleaving efficiency of complexes **1** and **2** has been assessed by their ability to convert supercoiled pBR 322 DNA from form I to form II (no form III is observed) by agarose gel electrophoresis. As shown in Figure 13, no distinct DNA cleavage was observed for the control in which the complex was absent (lane 1); however, with increasing concentration of the complexes (**1** and **2**), the amount of nicked DNA (form II) increases gradually whereas that of supercoiled DNA (form I) diminishes (lanes 2-5). Hence, the complexes exhibited excellent DNA cleavage activity in the absence of an external agent. Additionally, the amount of helical unwinding induced by the complex bound to SC DNA provides evidence for the intercalation mode of interaction between the complexes and DNA.[59] The nuclease activity of the complexes (**1** and **2**) can be estimated from the percentage of cleavage (C) (Table 6).

Protein binding studies

Fluorescence spectra

Interaction between the most abundant blood protein, that is, serum albumin, and complexes has attracted immense interest because of their structural homology with human serum albumin. To understand the mechanism of interaction between the test compounds (H_2L1, **1** and **2**) and BSA, fluorescence quenching experiments have been carried out. The fluorescence property of BSA arise from its intrinsic characteristics, mainly due to the presence of tryptophan and tyrosine residues.[60] Fluorescence titration studies have been performed using 1 μM BSA and varying the concentration of the compounds (0–20 μM) in the range 290–500 nm (λ_{ex} 280 nm, Fig. 14). The fluorescence intensity of BSA at 342 nm was quenched with a blue and red shifts by the ligand and the complexes respectively (85%, 4 nm, H_2L1; 94%, 9 nm, **1**; and 94%, 12 nm, **2**). The blue or red shift primarily arises due to the presence of the active site of the protein in a hydrophobic environment. It suggested that interaction is taking place between the compounds and BSA.[61] To have a deep insight into the quenching progression, quenching constant (K_q) was evaluated following Stern–Volmer equation using F^o/F *versus* [Q] plot (Fig. 15). Further, the equilibrium binding constant was evaluated using the following equation $\log[(F^o - F)/F] = \log K_b + n \log [Q]$ where K_b is binding constant of the compound with BSA and n is number of binding sites. From the log $(F^o - F)/F$ *versus* log [Q] plot (Fig. 16), the binding constant and the number of binding sites have been calculated. Evaluated values of the K_q, K_b, and n are gathered in Table 7. The estimated value of n (~1) strongly supported the existence of a single binding site in BSA. The values of K_b for these compounds further suggested that **2** interact with BSA rather strongly relative to other compounds under investigation. Further the interaction between **1** and BSA was confirmed by MALDI-TOF MS analysis. The mass of complex (**1**) bound BSA (Fig. S7) is very much higher than that of BSA alone (MW = 66,408), which supports the binding of complexes with BSA.[62]

UV-Vis absorption spectra

The absorption spectrum of BSA offers a simple and an easy means to explore the type of quenching. For a dynamic quenching appreciable change in absorption spectra of the fluorophore is not expected; in contrast, static quenching usually leads to perturbation of the fluorophore.[63] The absorption intensity of BSA increases with a small blue shift of about ~2 nm and suggested static interaction between BSA and the compounds (Fig. 17). The values of the binding constant are comparable with the reported data.[64]

Synchronous fluorescence spectra

To understand the structural changes of BSA due to the addition of the test compounds (H_2L1, **1** and **2**), we have measured synchronous fluorescence spectra of the compounds (Figs. 18 and 19). While increasing the concentration of the compounds, the intensity of emission corresponding to tyrosine (at 300 nm) was found to decrease in the magnitude of 87.0, 60.1 and 69.7% for compounds **1**, **2** and H_2L1 respectively without any shift in the emission wavelength. The tryptophan fluorescence emission showed significant decrease in the intensity (at 340 nm) of about 91.5, 83.1 and 70.6% for the compounds **1**, **2** and H_2L1 respectively, without any change in the position of the emission band. These results indicate that although the compounds affected the microenvironments of both tyrosine and tryptophan during the binding process, the effect is more pronounced toward tryptophan than tyrosine.

Cytotoxicity

The cytotoxicity results are summarized in Table 8 and Figs. 20 and 21. Generally the ligand (H_2L1) is poorly cytotoxic in all the tested cell lines. The trinuclear Cu(II) and Ni(II) self-assemblies exhibited significant cytotoxic effect in the low micromolar concentration. Notably, they are more cytotoxic than H_2L1 and cyclophosphamide toward the resistant A549 and MCF7 cell lines. The IC50 values for **1** are 22.36 and 10.0 μM against A549 and MCF7 cell lines respectively. *In vitro* cytoxicity of the complex **1** demonstrate that the complex have higher toxicity than previous reported copper complexes for both cancer cell lines (A549 and MCF7).[65] Complex **2** exhibited the IC50 values of 29.24 and 18.04 μM for the same cell lines. The high cytotoxicity of the complexes may originate from the strong hydrophobic interaction of the complexes with both DNA and protein.

Conclusions

Synthesis and characterization of bipodal 3,3,3′,3′-tetrabenzyl-1,1′-aroylbis(thioureas) and their metallamacrocyclic square planar Ni(II) and Cu(II) complexes are described. Metal to ligand stoichiometry of 2:2 and 3:3 can be achieved by using *meta* and *para* substituted ligands, respectively. The synthesized compounds are characterized by analytical and spectral (Mass, EPR/NMR, FT-IR and UV-Vis) techniques. The structures of the ligands (H_2L1 & H_2L2) and the complexes [**2** and **3**$(Py)_2$] have been confirmed by single crystal X-ray diffraction studies. The interaction of H_2L1, **1** and **2** with calf thymus (CT) DNA and bovine serum albumin (BSA) protein was investigated using UV-Visible and fluorescence spectroscopic methods. Absorption and emission spectral studies indicate that the complexes **1** and **2** interact with CT DNA and BSA protein more strongly than their parent ligand. DNA

unwinding study of **1** and **2** suggested intercalation mode of binding of complexes with DNA. Complexes **1** and **2** exhibited good cytotoxicity against A549 and MCF7 cancer cell lines. The IC50 values of the complexes (**1** and **2**) are comparable with that of cyclophosphamide.

Acknowledgements

N.S. thanks NITT for the fellowship. R.K. gratefully acknowledges DST for the financial support.

References

1 R, Richter, J. Sieler, R. Kohler, E. Hoyer, L. Beyer, I. Leban and L. Golic, *Z. Anorg. Allg. Chem*., 1989, **578**, 198.

2 (*a*) A. Rodenstein, R. Richter and R. Kirmse, *Z. Anorg. Allg. Chem*., 2007, **633**, 1713. (*b*) S. A. Bourne, O. Hallale and K. R. Koch, *Cryst. Growth Des*., 2005, **5**, 307. (*c*) A. Rodenstein, J. Griebel, R. Richter and R. Kirmse, *Z. Anorg. Allg. Chem*., 2008, **634**, 867.

3 (*a*) K. R. Koch, S. A. Bourne, A. Coetzee and J. Miller, *J. Chem. Soc*., *Dalton Trans*., 1999, **18**, 3157. (*b*) K. R. Koch, S. A. Bourne, A. Coetzee, J. Miller, and J. Bacsa, *J. Mol. Struct*., 2001, **561**, 185.

4 O. Hallale, S. A. Bourne and K. R. Koch, *New J. Chem*., 2005, **29**, 1416.

5 O. Hallale, S. A. Bourne and K. R. Koch, *Cryst. Eng. Comm*., 2005, **7**, 161.

6 A. N. Westra, S. A. Bourne and K. R. Koch, *Dalton Trans*., **2005**, 2916.

7 H. H. Nguyen, P. C. Thang, A. Rodenstein, A. R. Kirmse and Abram, *Inorg. Chem*., 2011, **50**, 590.

8 Q. Jiang, N. Xiao, P. Shi, Y. Zhu and Z. Guo, *Coord. Chem. Rev*., 2007, **251**, 1951.

9 (*a*) Y.-G. Fang, J. Zhang, S.-Y. Chen, N. Jiang, H.-H. Lin, Y. Zhang and X.-Q. Yu, *Bioorg. Med. Chem*., 2007, **15**, 696. (*b*) Y. Zhao, J. Zhu, W. He, Z. Yang, Y. Zhu, Y. Li, J. Zhang and Z. Guo, *Chem.–Eur. J*., 2006, **12**, 6621. (*c*) K. J. Humphreys, K. D. Karlin and S. E. Rokita, *J. Am. Chem. Soc*., 2002, **124**, 6009. (*d*) C. Tu, Y. Shao, N. Gan and Z. Guo, *Inorg. Chem*., 2004, **43**, 4761.

10 (*a*) J. Chen, X. Wang, Y. Shao, J. Zhu, Y. Zhu, Y. Li, Q. Xu and Z. Guo, A. *Inorg. Chem*., 2007, **46**, 3306. (*b*) J. L. Garcia-Gimenez, G. Alzuet, M. Gonzalez-Alvarez, A. Castineiras, M. Liu-Gonzalez and J. Borras, J. *Inorg. Chem*., 2007, **46**, 7178.

11 (*a*) P. R. Reddy and K. S. Rao, C*hem. Biodivers*., 2006, **3**, 231. (*b*) C. J. Burrows, and S. Rokita, *Acc. Chem. Res*., 1994, **27**, 295. (*c*) J. G. Muller, X. Chen, A. C. Dadiz, S. E. Rokita and C. J. Burrows, *J. Am. Chem. Soc*., 1992, **114**, 6407. (*d*) X. Chen, C. J. Burrows, and S. E. Rokita, *J. Am. Chem. Soc*., 1992, **114**, 322. (*e*) D. P. Mack and P. B. Dervan, *J. Am. Chem. Soc*. 1990, **112**, 4604. (*f*) K. Jeyalakshmi, N. Selvakumaran, N. S. P. Bhuvanesh, A. Sreekanth and R. Karvembu, *RSC Adv*., 2014, **4**, 17179.

12 (*a*) S. Zhang, Y. Zhu, C. Tu, H. Wei, Z. Yang, L. Lin, J. Ding, J. Zhang and Z. Guo, *J. Inorg. Biochem*., 2004, **98**, 2099. (*b*) V. Rajendiran, R. Karthik, M. Palaniandavar, H. S. Evans, V. S. Periyasamy, M. A. Akbarsha, B. S. Srinag and H. Krishnamurthy,

Inorg. Chem., 2007, **46**, 8208. (*c*) S. Mahadevan, and M. Palaniandavar, *Chem. Commun*., 1996, 2547. (*d*) S. Ramakrishnan, V. Rajendiran, M. Palaniandavar, V. S. Periasamy, M. A. Akbarsha, S. B Srinag and H. Krishnamurthy, *Inorg. Chem*., 2009, **48**, 1309. (*e*) R. Loganathan, S. Ramakrishnan, E. Suresh, A. Riyasdeen, M. A. Akbarsha and M. Palaniandavar, *Inorg. Chem*., 2012, **51**, 5512. (*f*) N. Selvakumaran, N. S. P. Bhuvanesh, A. Endo and R. Karvembu, R. *Polyhedron*, 2014, **75**, 95.

13 J. Liu, T. B. Lu, H. Deng, L. N. Ji, L.H. Qu and H. Zhou, *Trans. Met. Chem*., 2003, **28,** 116.

14 S. Anbu, M. Kandaswamy, S. Kamalraj, J. Muthumarry and B. Varghese, *Dalton Trans*., 2011, **40**, 7310.

15 X. Chen, J. Wang, S. Sun, J. Fan, S. Wu, J. Liu, S. Ma, L. Zhang and X. Peng, *Bioorg. Med. Chem. Lett*., 2008, **18**, 109.

16 O. Iranzo, A. Y. Kovalevsky, J. R. Morrow and J. P. Richard, *J. Am. Chem. Soc*., 2003, **125**, 1988.

17 C.-L. Liu, J.-Y. Zhou, Q.-X. Li, L.-J. Wang, Z.-R. Liao and H.-B. Xu, *J. Inorg. Biochem*. 1999, **75**, 233.

18 D. K. Chand, H. J. Schneider, J. A. Aguilar, F. Escarti, E. Garcia-Esspara and S. V. Luis, *Inorg. Chim. Acta*, 2001, **316**, 71.

19 K. J. Humphreys, K. D. Karlin and S. E. Rokita, *J. Am. Chem. Soc*., 2002, **124**, 8055.

20 (*a*) K. J. Humphreys, K. D. Karlin and S. E. Rokita, *J. Am. Chem. Soc*., 2001, **123**, 5588. (*b*) L. Li, N. N. Murthy, J. Tesler, L. N. Zakharov, G. P. A. Yap, A. L. Rheingold, K. D. Karlin and S. Rokita, *Inorg. Chem*., 2006, **45**, 7144.

21 M. A. Halcrow and G. Christou, *Chem. Rev*.,1994, **94**, 2421.

22 T. I. Doukov, T.M. Iverson, J. Seravalli, S.W. Ragsdale and C. L. Drennan. *Science*, 2002, **298**, 567.

23 R. K. Andrews, R. L. Blakely and B. Zerner, *Adv. Inorg. Biochem*., 1984, **6**, 245.

24 N. E. Dixon, P.W. Riddles, C. Gazzola, R. L. Blakely and B. Zerner, *Can. J. Biochem*., 1980, **58**, 1335.

25 P. A. Clark and D. E. Wilcox, *Inorg. Chem*., 1989, **28**, 1326.

26 K. Yamaguchi, F. Akagi, S. Fujinami, M. Suzuki, M. Shionoya and S. Suzuki, *Chem. Commun*., 2001, 375.

27 S. Anbu, M. Kandaswamy and B. Varghese, *Dalton Trans*., 2010, **39**, 3823.

28 S. Anbu, S. Shanmugaraju and M. Kandaswamy, *RSC Adv*., 2012, **2**, 5349.

29 G. L. Eichhorn and Y. A. Shin, *J. Am. Chem. Soc*., 1968, **90**, 7323.

30 P. M. Takahara, C. A. Frederick and S. J. Lippard, *J. Am. Chem. Soc*., 1996, **118**, 12309.

31 T. F. Kagawa, B. H. Geierstanger, A. H. J. Wang and P. S. Ho, *J. Biol. Chem*., 1991, **266**, 20175.

32 C. Santini, M. Pellei, V. Gandin, M. Porchia, F. Tisato, C. Marzano, *Chem. Rev*., 2014, **114**, 815.

33 J. Liu, H. Zhang, C. Chen, H. Deng, T. Lu and L. Ji, *Dalton Trans*., 2003, 114.

34 J. Liu, T. Zhang, T. Lu, L. Qu, H. Zhou, Q. Zhang and L. Ji, *J. Inorg. Biochem*., 2002, **91**, 269.

35 A. Anbu, M. Kandaswamy, P. Suthakaran, V. Murugan, B. Varghese, *J. Inorg. Biochem*., 2009, **103**, 401.

36 S. Anbu and M. Kandaswamy, *Polyhedron*, 2011, **30**, 123.

37 D. Lahiri, T. Bhowmick, B. Pathak, O. Shameema, A. K. Patra, S. Ramakumar and A. R. Chakravarty, *Inorg. Chem*., 2009, **48**, 339.

38 (*a*) S. Anbu, M. Kandaswamy and M. Selvaraj, *Polyhedron*, 2012, **33**, 1. (*b*) S. Anbu, M. Kandaswamy, P. S. Moorthy, M. Balasubramanian and M. N. Ponnuswamy, *Polyhedron*, 2009, **28**, 49. (c) S. Anbu, M. Kandaswamy, *Inorg. Chim. Acta*, 2012, **385**, 45.

39 FRAMBO v. 4.1.05; ; APEX2 v2012.10-0 "*Program for Data Collection on Area Detectors*" BRUKER-Nonius Inc., 5465 East Cheryl Parkway, Madison, WI 53711-5373, USA.

40 G. M. Sheldrick, "Cell_Now (version 2008/1): *Program for Obtaining Unit Cell Constants from Single Crystal Data*", University of Göttingen, 2008.

41 APEX2 "*Program for Data Collection and Integration on Area Detectors*" BRUKER AXS Inc., 5465 East Cheryl Parkway, Madison, WI 53711-5373 USA.

42 G. M. Sheldrick, "SADABS (version 2008/1): *Program for Absorption Correction for Data from Area Detector Frames*", University of Göttingen, 2008.

43 G. M. Sheldrick, *Acta Cryst*., 2008, A**64**, 112.

44 O. V. Dolomanov, L. J. Bourhis, R. J. Gildea, , J. A. K. Howard and H. Puschmann, *J. Appl. Cryst*., 2009, **42**, 339.

45 A. L. Spek, *J. Appl. Cryst*., 2003, **36**, 7.

46 J. A. Simpson, K. H. Cheeseman, S. E. Smith and R. T. Dean, *Biochem. J.*, 1988, **54**, 519.

47 C. Rajput, R. Rutkaite, L. Swanson, I. Haq and J. A. Thomas, *Chem.–Eur. J.*, 2006, **12**, 4611.

48 G. Cohen and H. Eisenberg, *Biopolymers*, 1969, **8**, 45.

49 M. S. Deshpande, A. A. Kumbhar, A. S. Kumbhar, M. Kumbhakar, H. Pal, U. B. Sonawane and R. R. Joshi *Bioconj. Chem*., 2009, **20**, 447.

50 T. J. Mossman, *Immunol. Methods*, 1983, **65**, 55.

51 T. K. Goswami, B. V. Chakravarthi, M. Roy, A. A. Karande and A. R. Chakravarty, *Inorg. Chem*., 2011, **50**, 8452.

52 A. B. P. Lever, *Inorganic Electronic Spectroscopy*, 2nd Ed., Elsevier, Amsterdam, 1984.

53 D. J. Che, G. Li, X. L. Yao, Y. Zhu, D. P. Zhou, *J. Chem. Soc., Dalton Trans*., 1999, 2683.

54 L. Yang, D. R. Powell and R. P. Houser, *Dalton Trans*. 2007, 955.

55 J. R. Lakowicz and G. Weber, *Biochemistry*, 1973, **12**, 4161.

56 K. S. Ghosh, B. K. Sahoo, D. Jana and S. Dasgupta, *J. Inorg. Biochem*., 2008, **102**, 1711.

57 (*a*) D. S. Raja, N. S. P. Bhuvanesh and K. Natarajan, *Dalton Trans*. 2012, **41**, 4365. (*b*) E. Ramachandran, D. S. Raja, N. S. P. Bhuvanesh and K. Natarajan, *Dalton Trans*. 2012, **41**, 13308. (*c*) D. S. Raja, N. S. P. Bhuvanesh and K. Natarajan, *Eur. J. Med. Chem*. 2012, **47**, 73.

58 C. V. Kumar and E. H. Asuncion, *J. Am. Chem. Soc*., 1993, **115**, 8547.

59 J. Liu, W. J. Zheng, S. Shi, C. P. Tan, J. C. Chen, K. C. Zheng and L. N. Ji, *J. Inorg. Biochem*., 2008, **102**, 193–202.

60 K. A. Z. Osama and I. K. A. S. Othman, *J. Am. Chem. Soc*., 2008, **130**, 10793.

61 (*a*) P. Krishnamoorthy, P. Sathyadevi, A. H. Cowley, R. Butorac and N. Dharmaraj, *Eur. J. Med. Chem*., 2011, **46,** 3376. (*b*) P. Sathyadevi, P. Krishnamoorthy, R. Butorac, A. H. Cowley, N. S. P. Bhuvanesh and N. Dharmaraj, *Dalton Trans*., 2011, **40**, 9690. (*c*) P. Krishnamoorthy, P. Sathyadevi, A. H. Cowley, R. Butorac and N. Dharmaraj, *Dalton Trans*., 2012, **41**, 6842.

62 S. K. Leung, K. Y. Kwok, K. Y. Zhang, and K. K. Wing Lo, *Inorg. Chem*., 2010, **49**, 4984.

63 (*a*) J. R. Lakowicz, *Fluorescence Quenching: Theory and Applications. Principles of Fluorescence Spectroscopy*, Kluwer Academic/Plenum Publishers, New York, 1999, 53127. (*b*) X. Z. Feng, Z. Yang, L. J. Wang and C. Bai, *Talanta*, 1998, **47**, 1223.

64 A. Patra, T. K. Sen, A. Ghorai, G. T. Musie, S. K. Mandal, U. Ghosh and M. Bera, *Inorg. Chem*., 2013, **52**, 2880.

65 P. Kumar, S. Gorai, M. Kumar Santra, B. Mondal and D. Manna, *Dalton Trans*., 2012, **41**, 7573.

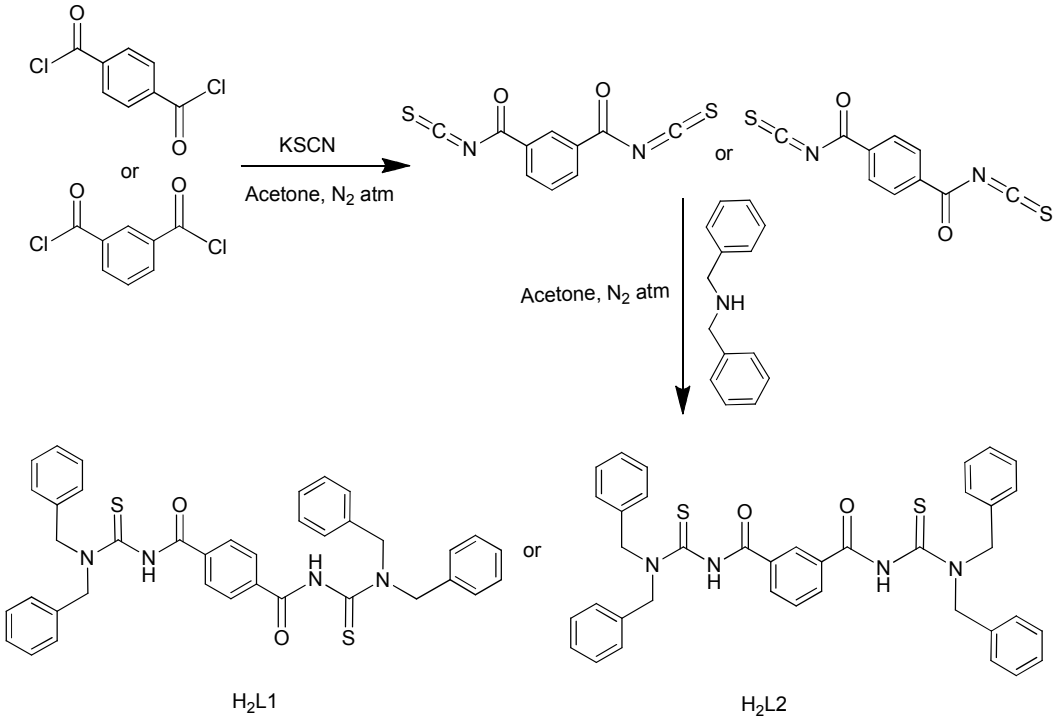

Scheme 1 Synthesis of bipodal ligands.

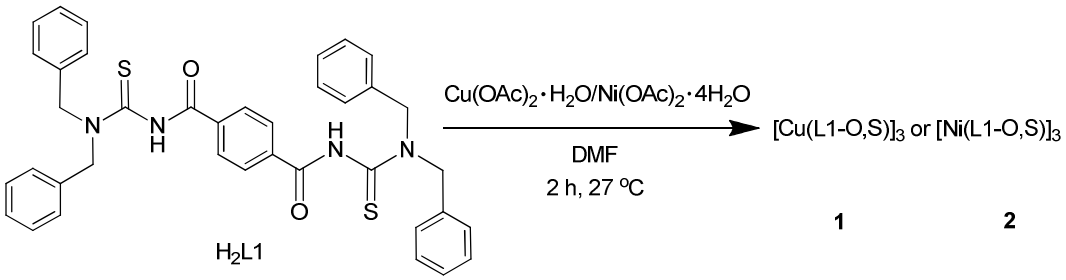

Scheme 2 Synthesis of 3:3 self assembled Cu(II) and Ni(II) complexes.

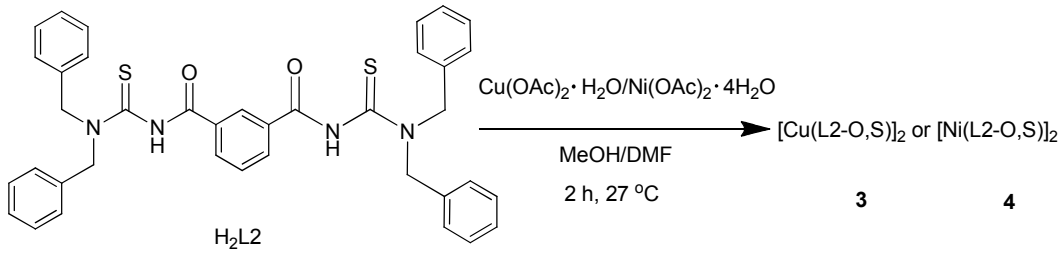

Scheme 3 Synthesis of 2:2 self assembled Cu(II) and Ni(II) complexes.

Table 1 Crystal data and structure refinement for ligands

Ligand	H_2L1	H_2L2
Empirical formula	$C_{44}H_{49}N_6O_{4.50}S_2$	$C_{38}H_{34}N_4O_2S_2$
Formula weight	798.01	642.81
Temperature (K)	150(2)	110(2)
Wavelength (Å)	0.71073	0.71073
Crystal system	Triclinic	Orthorhombic
Space group	*P*-1	$P2_12_12_1$
Unit cell dimensions		
a (Å)	9.660(4)	6.4932(6)
b (Å)	10.747(5)	22.720(2)
c (Å)	10.981(5)	23.008(2)
α (°)	81.433(5)	90
β (°)	68.491(5)	90
γ (°)	84.688(5)	90
Volume ($Å^3$)	1047.9(8)	3394.3(5)
Z	1	4
Density (calculated)	1.265 Mg/m^3	1.258 Mg/m^3
Absorption coefficient	0.178 mm^{-1}	0.196 mm^{-1}
F(000)	423	1352
Crystal size (mm^3)	0.50 × 0.20 × 0.20	0.52 × 0.41 × 0.13
Theta range for data collection (°)	1.92 to 27.50	2.52 to 27.41
Index ranges	-12<=*h*<=12, -13<=*k*<=13, -14<=*l*<=14	-8<=*h*<=8, -29<=*k*<=29, -29<=*l*<=29
Reflections collected	12107	37645
Independent reflections	4726 [R(int) = 0.0297]	7693 [R(int) = 0.0401]
Completeness to theta =27.49°/60°	98.2%	99.6%
Absorption correction	Semi-empirical from equivalents	Semi-empirical from equivalents
Max. and min. transmission	0.9653 and 0.9163	0.9749 and 0.9048
Refinement method	Full-matrix least-squares on F^2	Full-matrix least-squares on F^2
Data / restraints / parameters	4726 / 0 / 264	7693 / 0 / 415
Goodness-of-fit on F^2	1.045	1.026
Final R indices [I>2σ(*I*)]	R1 = 0.0394, wR2 = 0.1039	R1 = 0.0370, wR2 = 0.0811
R indices (all data)	R1 = 0.0448, wR2 = 0.1089	R1 = 0.0433, wR2 = 0.0840
Largest diff. peak and hole ($e.Å^{-3}$)	0.713 and -0.405	0.328 and -0.346

Table 2 Crystal data and structure refinement for complexes

Complex	**2**	**3**$(Py)_2$
Empirical formula	$C_{114}H_{96}N_{12}Ni_3O_6S_6$	$C_{111}H_{99}Cu_2N_{15}O_4S_4$
Formula weight	2098.52	1962.37
Temperature (K)	110(2) K	110.15 K
Wavelength (Å)	1.54178	0.71073
Crystal system	Monoclinic	Monoclinic
Space group	$P2_1/n$	$P_12_1/c1$
Unit cell dimensions		
a (Å)	14.2692(7)	10.901(2)
b (Å)	36.2013(17)	38.112(8)
c (Å)	20.1957(10)	12.697(3)
α (°)	90	90
β (°)	109.057(2)	114.672(2)
γ (°)	90	90
Volume (Å^3)	9860.6(8)	4793.5(17)
Z	4	2
Density (calculated)	1.414 Mg/m^3	1.360 Mg/m^3
Absorption coefficient	2.365 mm^{-1}	0.595 mm^{-1}
F(000)	4368	2048
Crystal size (mm^3)	0.18 × 0.01 × 0.01	0.23 × 0.13 × 0.08
Theta range for data collection (°)	2.44 to 57.50	1.844 to 27.501
Index ranges	-15<=h<=14, -39<=k<=39, -22<=l<=22	-14<=h<=14, -49<=k<=49, -16<=l<=16
Reflections collected	86107	66701
Independent reflections	13148 [R(int) = 0.1170]	10961 [R(int) = 0.0400]
Completeness to theta =27.49°/60 °	97.2%	100.0%
Absorption correction	Semi-empirical from equivalents	Semi-empirical from equivalents
Max. and min. transmission	0.9767 and 0.6755	0.7456 and 0.7013
Refinement method	Full-matrix least-squares on F^2	Full-matrix least-squares on F^2
Data / restraints / parameters	13148 / 0 / 1270	10961 / 0 / 615
Goodness-of-fit on F^2	1.016	1.051
Final R indices [I>2σ(I)]	R1 = 0.0577, wR2 = 0.1227	R1 = 0.0355, wR2 = 0.0799
R indices (all data)	R1 = 0.0997, wR2 = 0.1388	R1 = 0.0456, wR2 = 0.0851
Largest diff. peak and hole (e.Å^{-3})	0.576 and -0.356	0.651 and -0.392

Table 3 Important bond lengths (Å) and angles (°) of ligands

	H_2L1	H_2L2
S(1)–C(1)	1.6710(14)	1.6795(19)
O(1)–C(16)	1.2207(15)	1.214(2)
N(1)–C(1,15)	1.3299(17)	1.322(2)
N(1)–C(2,8)	1.4734(15)	1.473(2)
N(2)–C(16)	1. 3740(10)	1. 379(2)
N(2)–C(1,15)	1.4230(15)	1.407(2)
N(2)–H(2)	0.9000	0.8800
C(1,15)–N(1)–C(2,8)	121.21(11)	120.85(15)
C(1,15)–N(1)–C(9,1)	124.22(10)	124.6(15)
C(2,8)–N(1)–C(9,1)	114.07(10)	114.55(13)
C(16)–N(2)–H(2)	120.02	118.8
O(2,1)–C(23,16)–N(3,2)	122.53 (11)	122.79(17)
O(2,1)–C(23,16)–C(19,17)	121.08(11)	122.77(17)
N(4,1)–C(24, 15)–S(2,1)	126.23(9)	124.55(14)
N(3,2)–C(24,15)–S(2,1)	117.95(9)	117.86(12)

Table 4 Important bond lengths (Å) and angles (°) of complexes

	2		**3**$(Py)_2$
Ni(1)–O(1)	1.864(3)	Cu(1)–O(1)	1.9680(12)
Ni(1)–S(1)	2.1316(15)	Cu(1)–S(1)	2.2638(6)
O(1)–C(1)	1.259(5)	O(1)–C(2)	1.253(2)
S(1)–C(2)	1.711(5)	S(1)–C(1)	1.7263(18)
N(1)–C(1)	1.833(6)	N(1)–C(1)	1.338(2)
N(1)–C(2)	1.344(6)	N(1)–C(2)	1.326(2)
N(2)–C(2)	1.355(6)	Cu(1)–N(2)	2.2275(16)
O(1)–Ni(1)–O(2F)	85.35(14)	S(1)–Cu(1)–S(2)#1	87.36(2)
O(1)–Ni(1)–S(1)	95.10(11)	O(1)–Cu(1)–S(1)	92.52(4)
O(2F)–Ni(1)–S(1)	175.89(12)	O(1)–Cu(1)–S(2)#1	163.55(4)
O(1)–Ni(1)–S(2F)	172.17(12)	O(2)#1–Cu(1)–S(1)	167.52(4)
S(1)–Ni(1)–S(2F)	83.63(3)	O(2)#1–Cu(1)–O(1)	85.14(5)
O(2F)–Ni(1)–S(2F)	96.48(11)	O(1)–Cu(1)–N(2)	95.22(6)
C(2)–S(1)–Ni(1)	109.41(17)	C(1)–S(1)–Cu(1)	101.38(6)
C(1)–O(1)–Ni(1)	131.9(3)	C(2)–O(1)–Cu(1)	128.57(11)

#1 -x, -y+1, -z; Symmetry transformations used to generate equivalent atoms

Table 5 DNA binding constant (K_b), quenching constant (K_q) and apparent binding constant (K_{app}) values

Compound	K_b (M^{-1})	K_q (M^{-1})	K_{app} (M^{-1})
H_2L1	1.52×10^4	2.94×10^4	1.47×10^6
1	1.98×10^4	3.87×10^4	1.94×10^6
2	2.38×10^4	3.45×10^4	1.73×10^6

Table 6 Self-activated cleavage data of SC pBR 322 DNA (20 μM) by complexes **1** and **2** (0-100 μM) for an incubation time of 2 h

Lane No.	Reaction conditions	Percentage of cleavage (C) (%)	
		SC	NC
1	DNA control	95.27	4.73
2	DNA + **1** (50 μM)	18.56	81.44
3	DNA + **2** (50 μM)	13.44	86.56
4	DNA + **1** (100 μM)	14.78	85.22
5	DNA + **2** (100 μM)	12.36	87.61

Table 7 Protein binding constant (K_b), quenching constant (K_q) and number of binding site (n) values

Compound	K_b (M^{-1})	K_q (M^{-1})	n
H_2L1	1.64×10^8	6.42×10^5	1.66
1	2.79×10^9	1.39×10^6	1.54
2	4.88×10^9	1.23×10^6	1.81

Table 8 *In vitro* cytotoxicity of the complexes in MCF7 and A549 cancer cell lines

Compound	IC50 (μM)	
	A549	MCF7
1	22.36	10.0
2	29.24	18.04
Cyclophosphamide	41.84	11.89

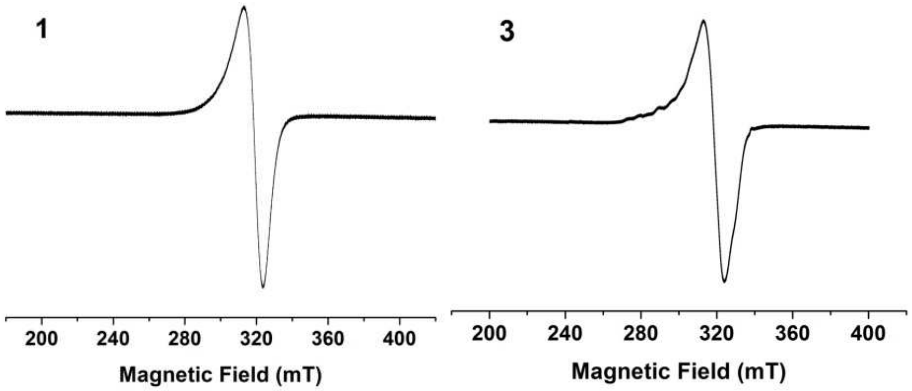

Fig. 1 X-Band EPR spectra of **1** and **3** in frozen state (ν = 9.78 GHz).

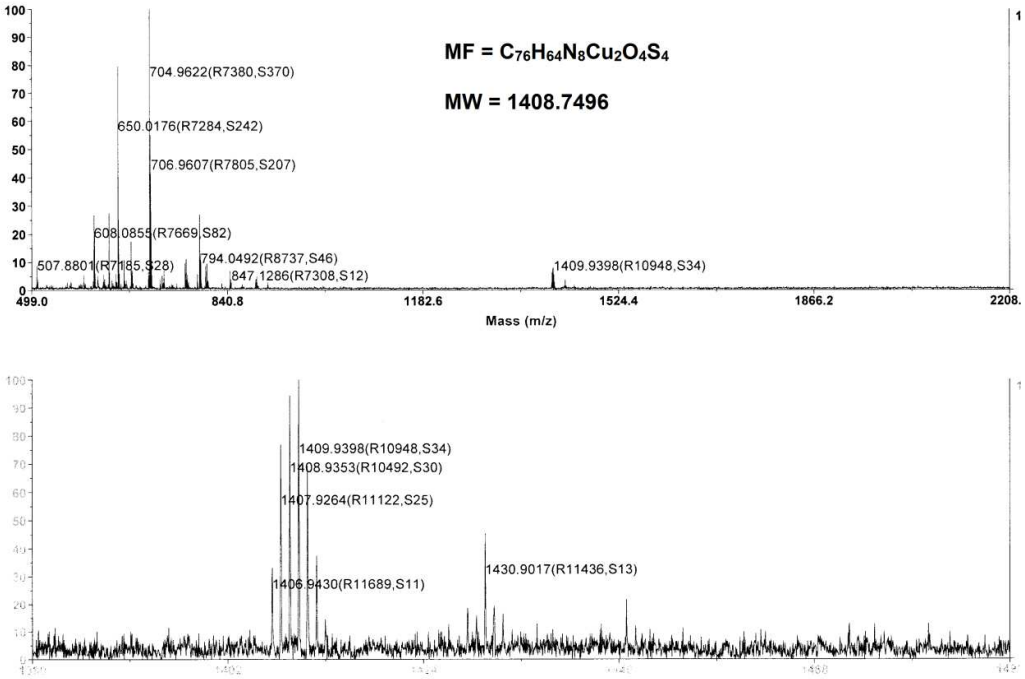

Fig. 2 MALDI-MS spectrum of **3**.

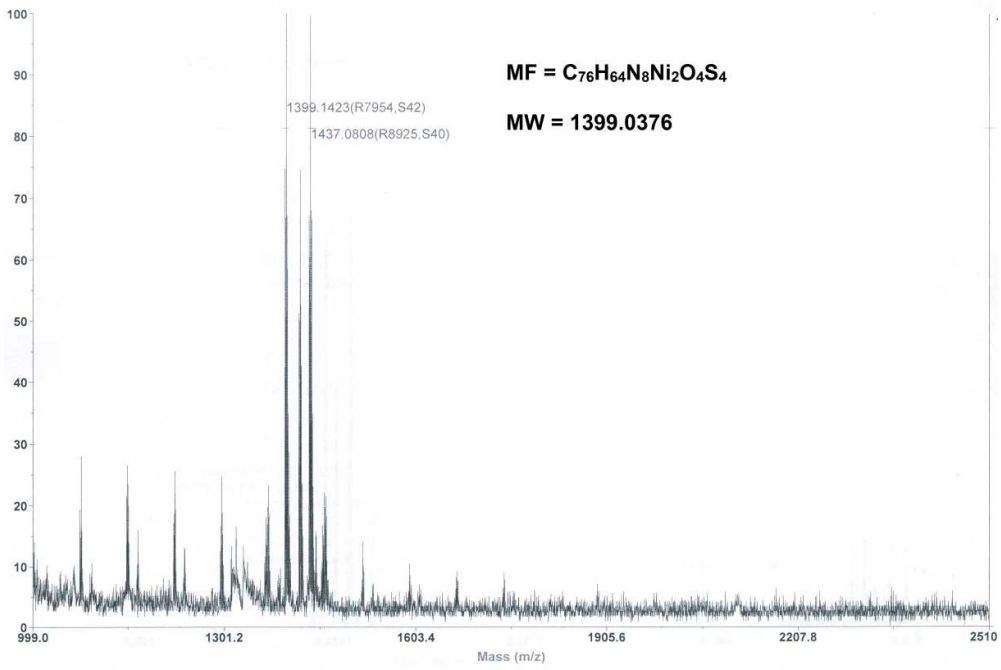

Fig. 3 MALDI-MS spectrum of **4**.

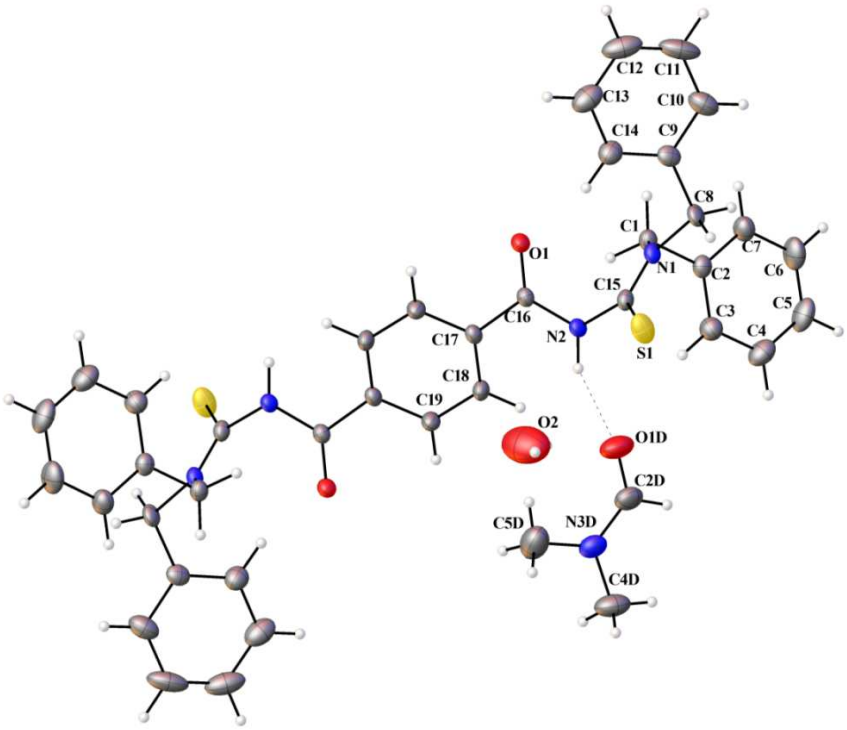

Fig. 4 Thermal ellipsoidal plot of H_2L1.

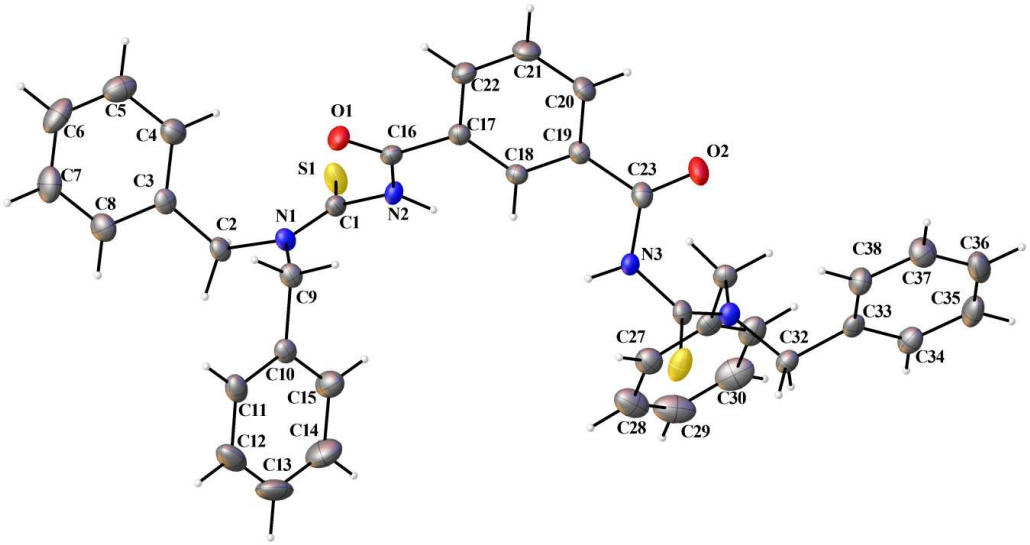

Fig. 5 Thermal ellipsoidal plot of H_2L2.

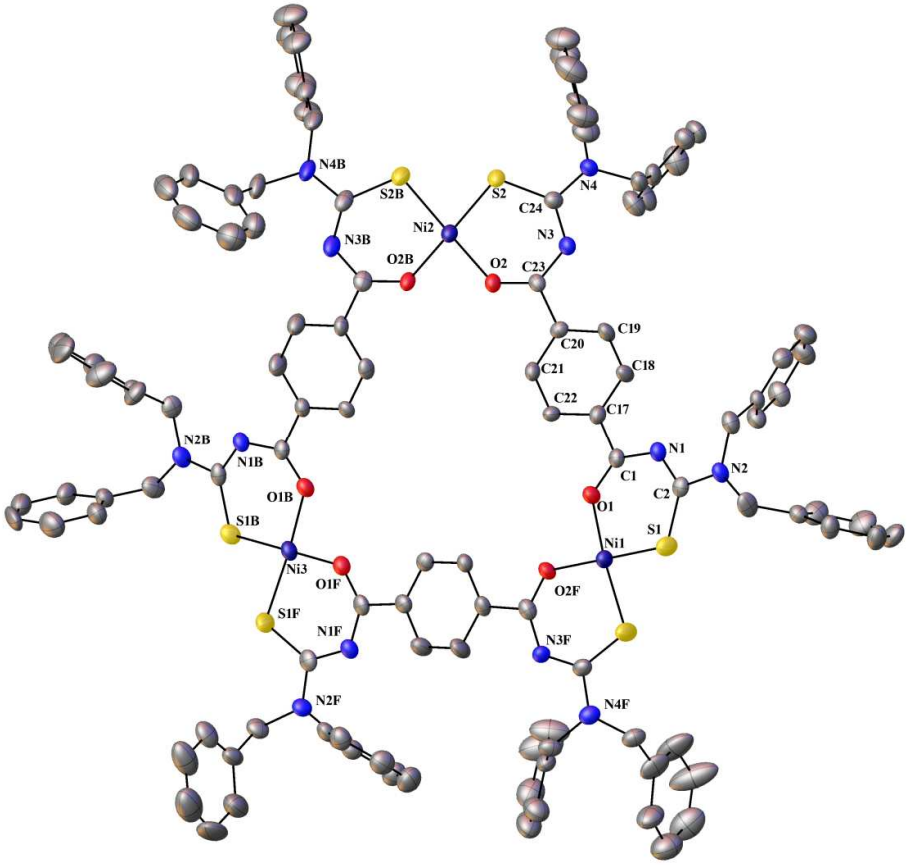

Fig. 6 Thermal ellipsoidal plot of **2**.

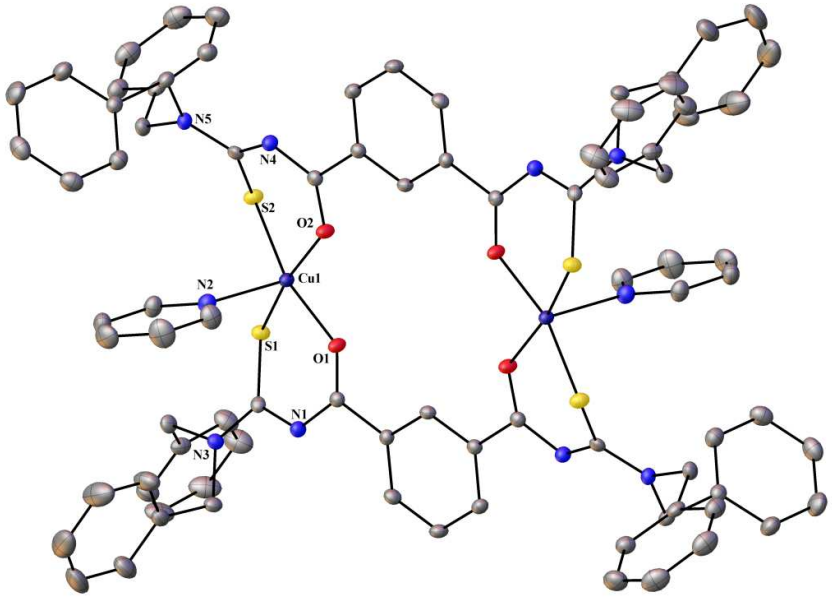

Fig. 7 Thermal ellipsoidal plot of **3**$(Py)_2$.

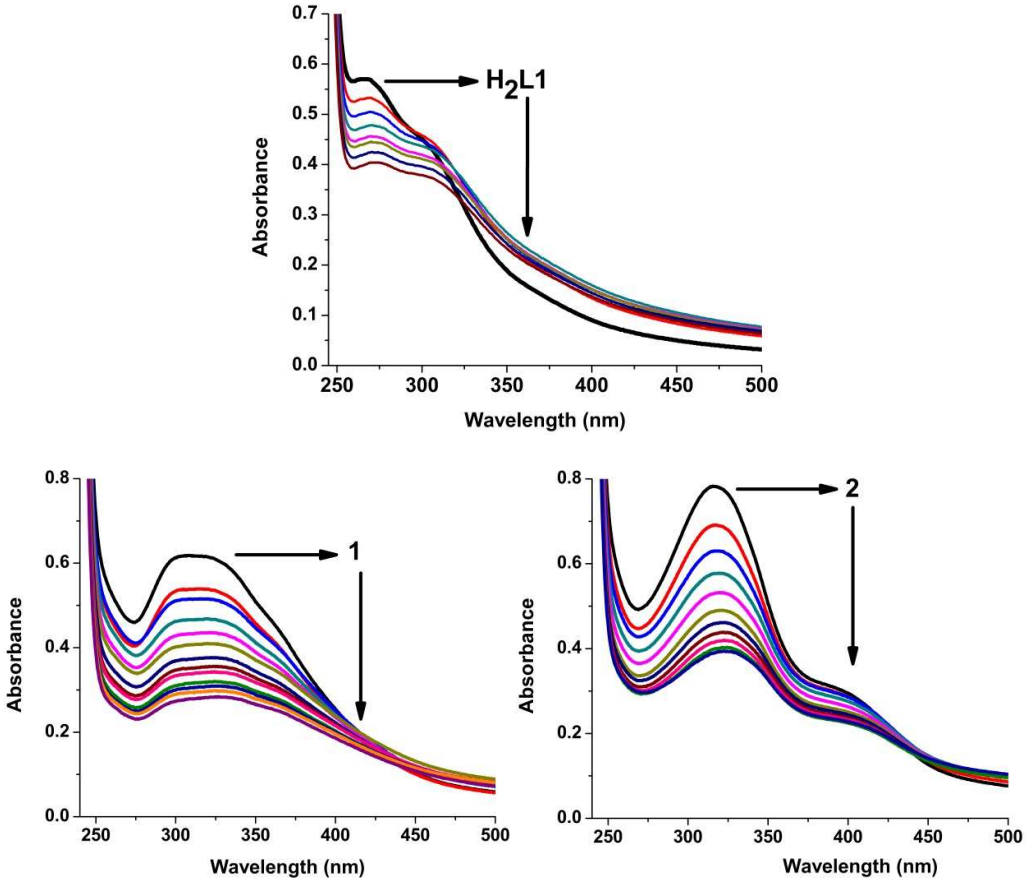

Fig. 8 Absorbance titrations of H_2L1, **1** and **2** (5 μM) with CT DNA (0-50 μM).

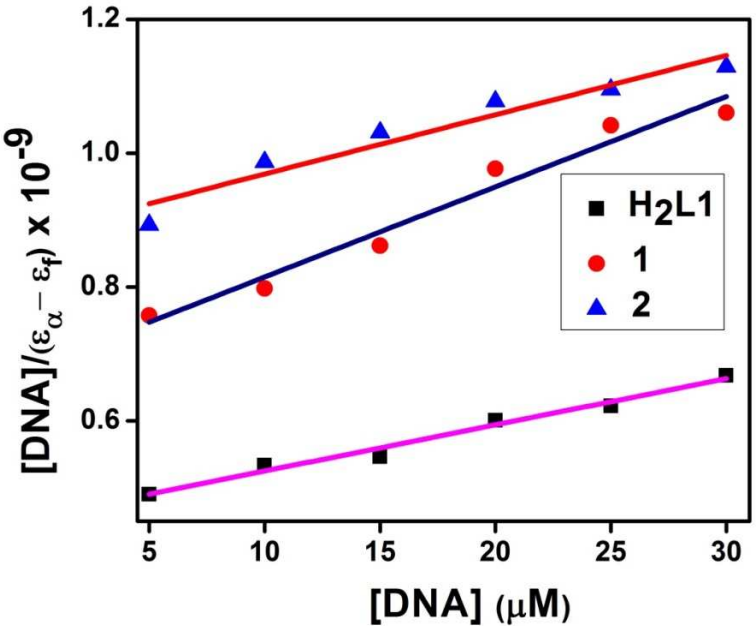

Fig. 9 Stern-Volmer plots of absorbance titrations of H_2L1, **1** and **2** with CT DNA.

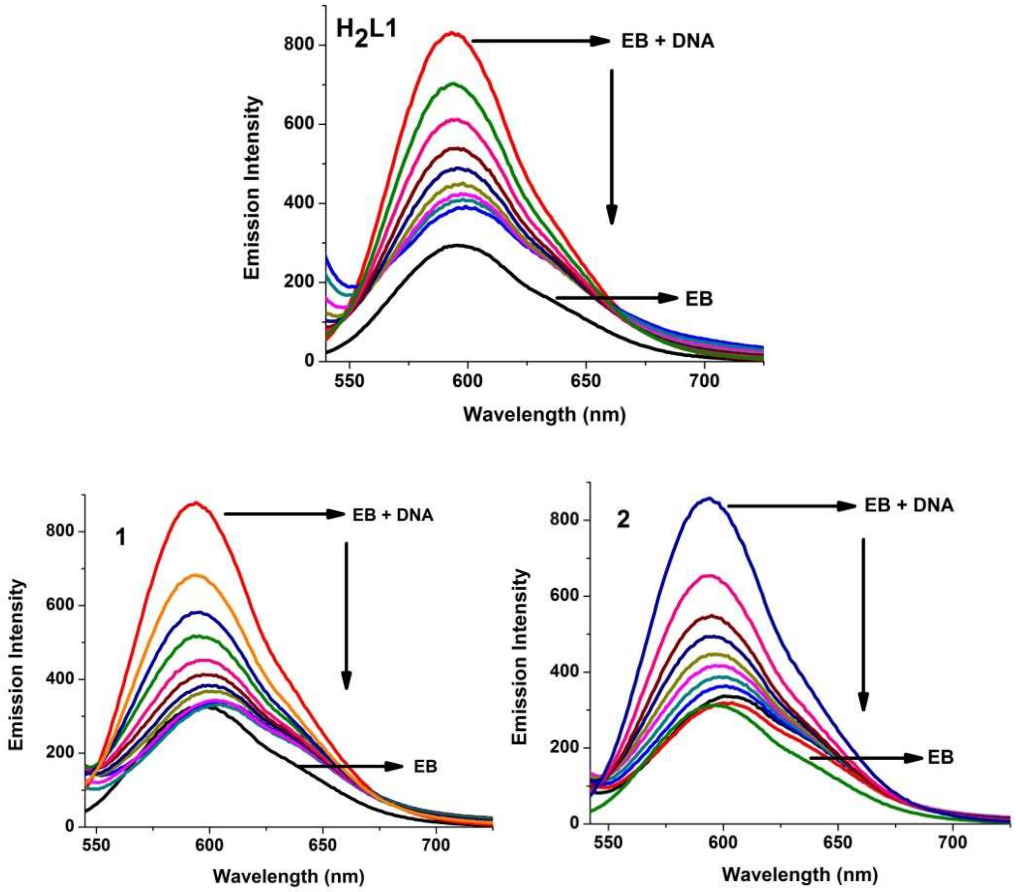

Fig. 10 Fluorescence titrations of H_2L1, **1** and **2** (0-50 μM) with EB bounded CT DNA (5 μM).

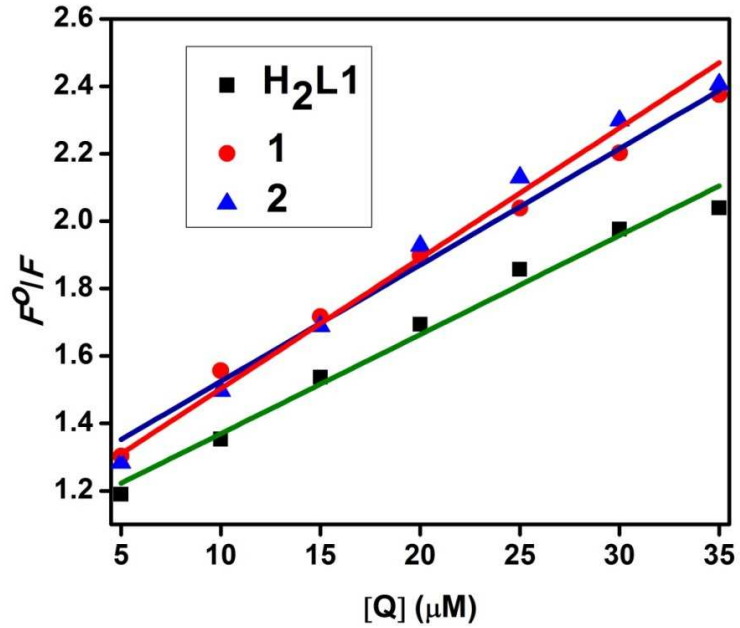

Fig. 11 Stern-Volmer plots of fluorescence titrations of H_2L1, **1** and **2** with CT DNA.

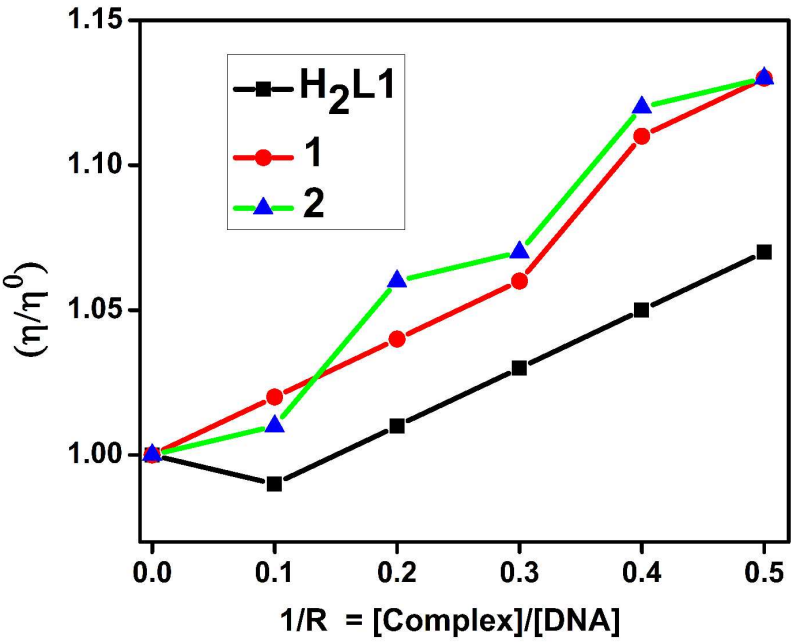

Fig. 12 Effect of the compounds (H_2L1, **1** and **2**) on the viscosity of CT DNA (0.5 M).

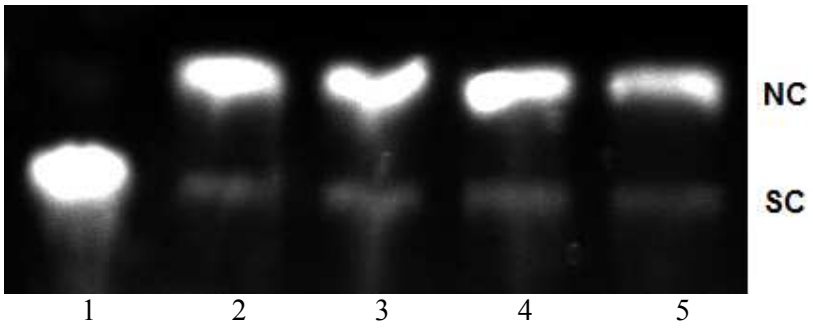

Fig. 13 Cleavage of supercoiled pBR322 DNA (20 μM) by complexes **1** and **2** in a buffer containing 2% DMF : 5 mM Tris HCl/50 mM NaCl at pH = 7.2 and 37 °C with an incubation time of 2 h. Lane 1, DNA; lane 2, DNA + **1** (50 μM); lane 3, DNA + **2** (50 μM); lane 4, DNA + **1** (100 μM); lane 5, DNA + **2** (100 μM). Forms SC and NC are supercoiled and nicked circular DNA, respectively.

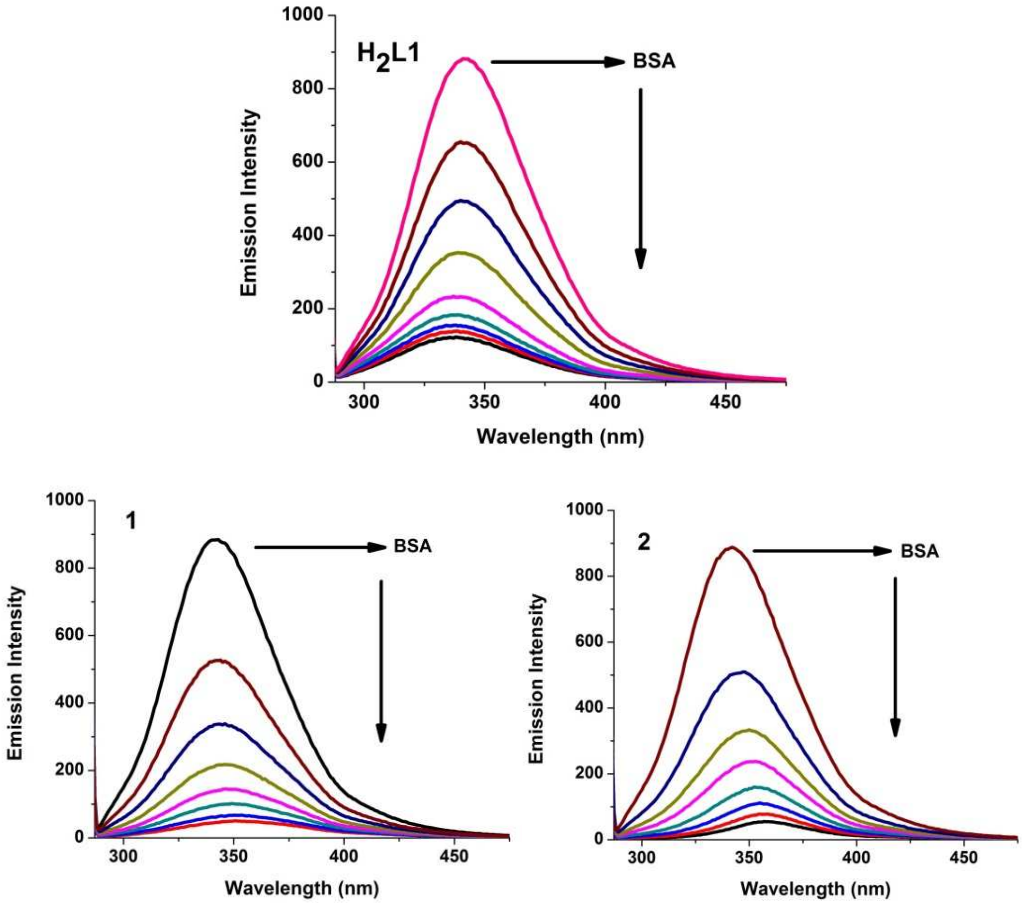

Fig. 14 Fluorescence titrations of H_2L1, **1** and **2** (0-20 μM) with BSA (1 μM).

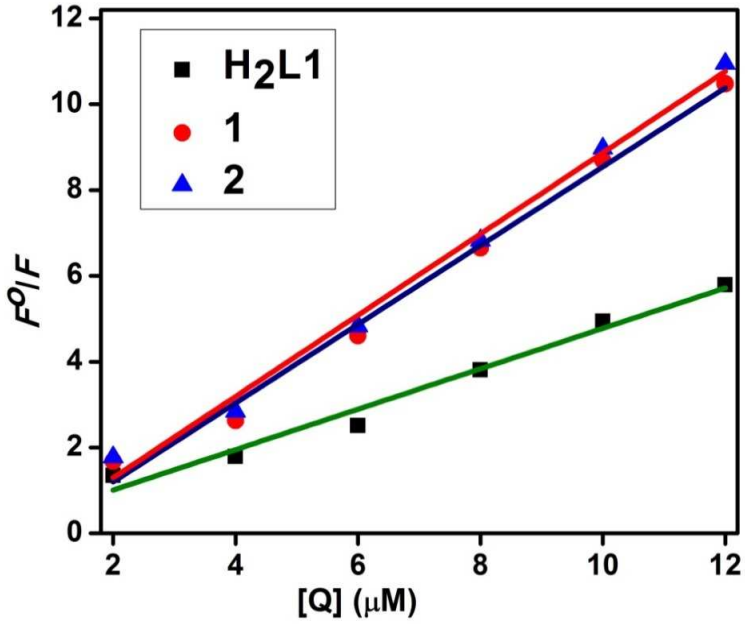

Fig. 15 Stern-Volmer plots of the fluorescence titrations of H_2L1, **1** and **2** with BSA.

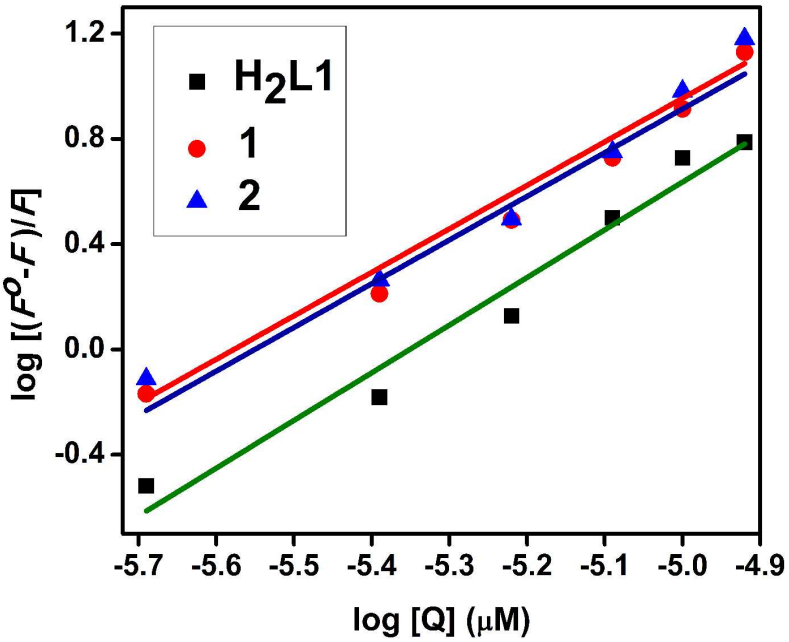

Fig. 16 Plot of log[Q] *vs*. log[$(F^0 - F)/F$].

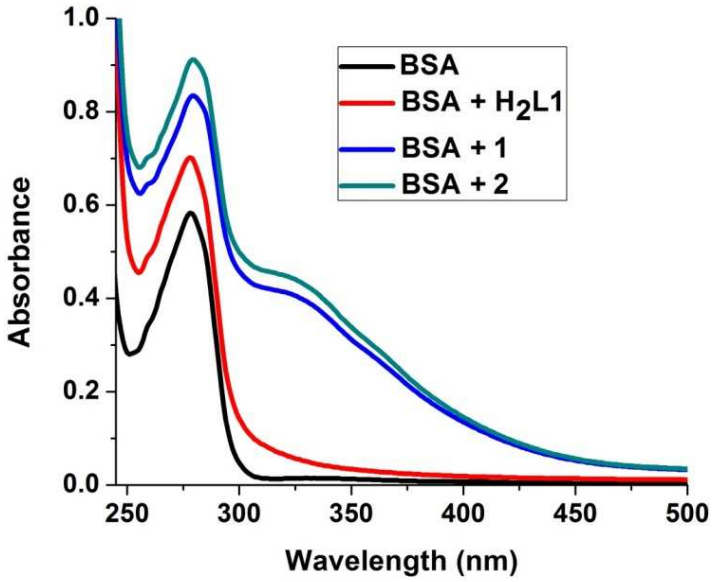

Fig. 17 Absorbance titrations of H_2L1, **1** and **2** with BSA.

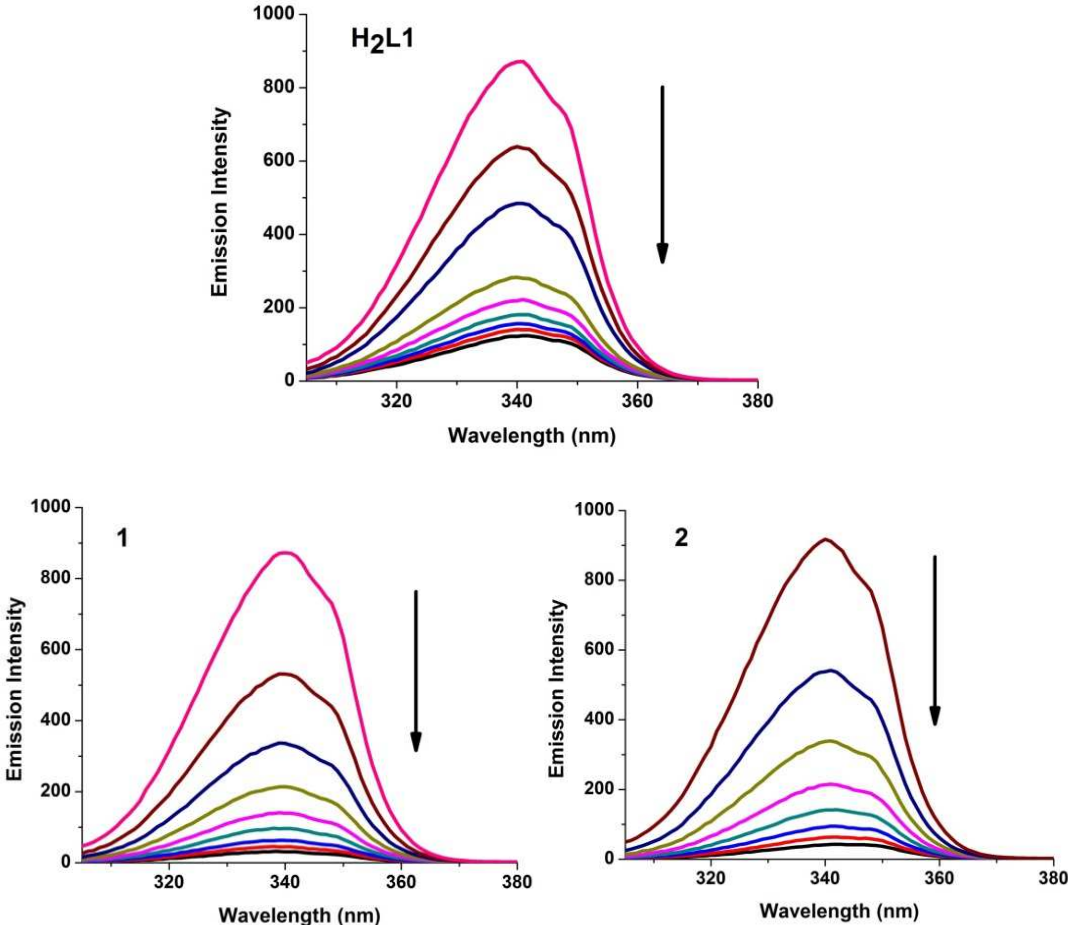

Fig. 18 Synchronous spectra of BSA (1μM) as a function of concentration of H_2L1, **1** and **2** (0-20 μM) with $\Delta\lambda$ = 60 nm.

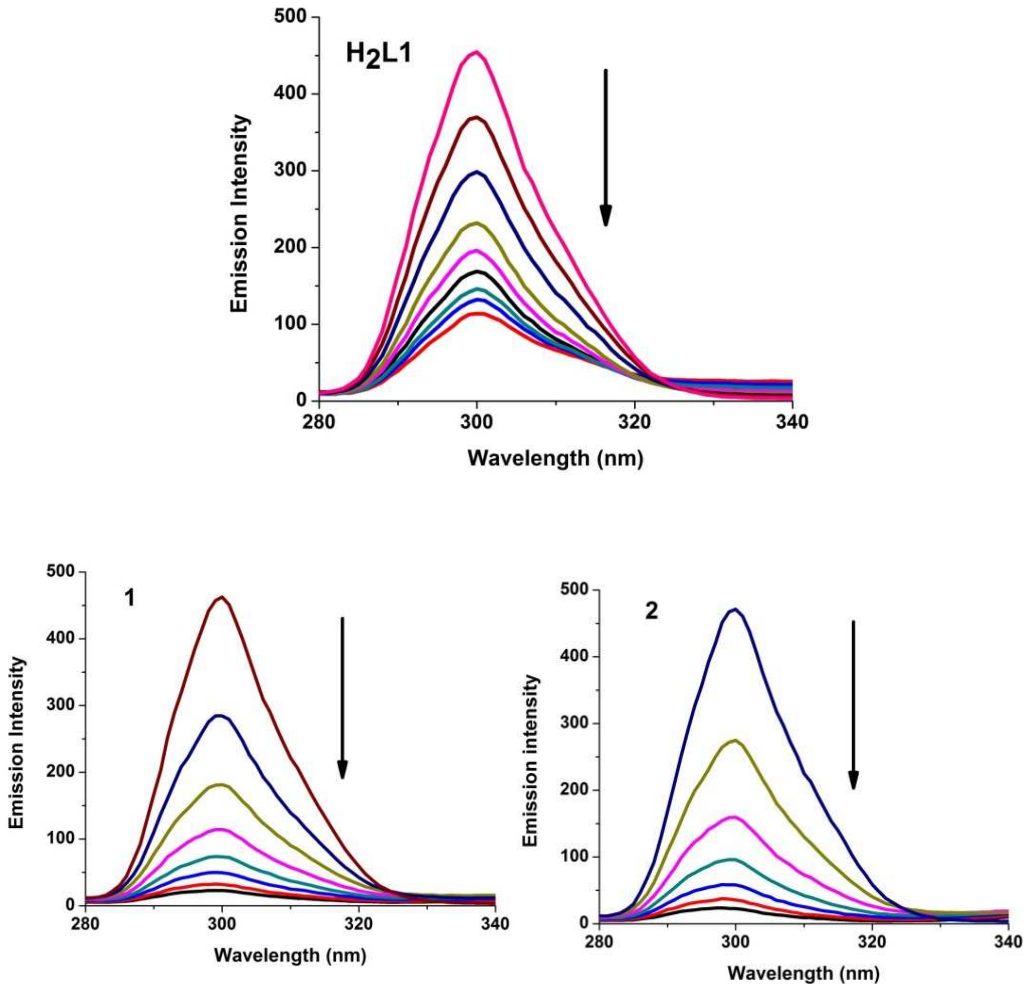

Fig. 19 Synchronous spectra of BSA (1μM) as a function of concentration of H_2L1, **1** and **2** (0-20 μM) with $\Delta\lambda$ = 15 nm.

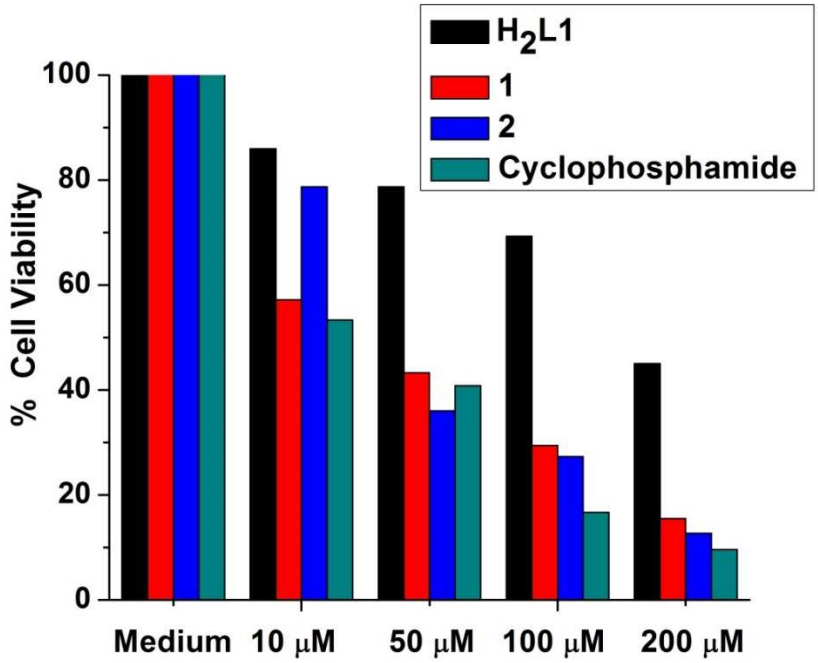

Fig. 20 Cytotoxicity of H_2L1, **1** and **2** after 24 h incubation on A549 cell lines.

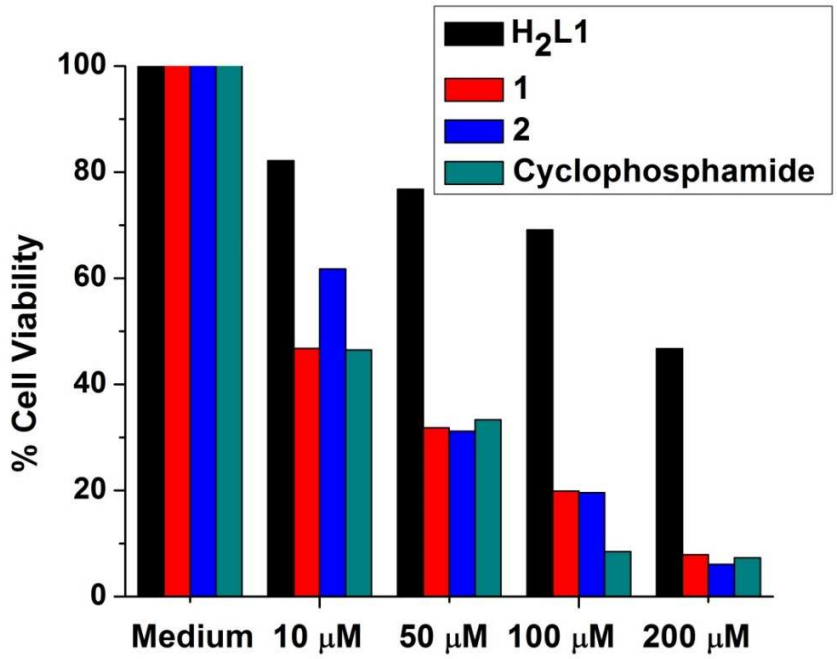

Fig. 21 Cytotoxicity of H_2L1, **1** and **2** after 24 h incubation on MCF7 cell lines.